

A semi-analytical matrix formalism for stress singularities in anisotropic multi-material corners with frictional boundary and interface conditions

María A. Herrera-Garrido, Vladislav Mantič^{*}, Alberto Barroso

Grupo de Elasticidad y Resistencia de Materiales, Escuela Técnica Superior de Ingeniería, Universidad de Sevilla, Camino de los Descubrimientos, s/n, Sevilla, 41092, Spain

ARTICLE INFO

Keywords:

Corner singularity
Interface crack
Singularity exponent
Anisotropic linear elastic material
Frictional contact
Stroh formalism

ABSTRACT

A new general semi-analytic procedure for the characterisation of singular asymptotic elastic states in the vicinity of the apex of linearly elastic anisotropic multi-material corners, including frictional contact, is developed and tested. The corners can consist of any finite number of homogeneous wedges defined by polar sectors. The variability of configurations covered is enormous as frictional contact can be considered on one or more outer boundary surfaces or interfaces, in addition to a large variety of homogeneous boundary conditions and perfect bonding or frictionless sliding interface conditions between wedges in the corner. The Coulomb rate-independent and dry frictional contact law is assumed. One of the novelties is that, in addition to the singularity exponent λ , the angle ω of the friction tangential stress vector on each frictional contact surface is an a priori unknown to be determined by solving a nonlinear corner eigensystem. The procedure, which considers power-law stress singularities, is based on the Stroh formalism of anisotropic elasticity, assuming generalised plane strain (2.5D) conditions, and on the semi-analytic matrix formalism for wedge transfer-matrices and boundary and interface condition matrices. This makes it, firstly, very suitable for computational implementations, secondly, very efficient especially in cases with several perfectly bonded homogeneous wedges, and, thirdly, very accurate due to its fully semi-analytic nature. The code developed is tested by solving a large variety of examples, comparing the present results with those obtained by solving closed-form corner-eigenequations deduced by previous authors for specific useful practical configurations, confirming the extremely high accuracy of the present code in the computation of λ and ω . The differences observed in some cases with anisotropic materials are explained by the fact that some of the previous authors did not take the true 3D Coulomb friction law into account.

1. Introduction

Friction has numerous implications in many areas of science and technology, it is an inherent phenomenon in the operation of mechanical systems where structural elements are in contact with each other, and is responsible for significant energy loss and wear. Frictional contact is often associated with stress concentrations or stress singularities with unbounded stresses, e.g., in material forming with frictional contact between the workpiece and the tool, punch indentation, fretting fatigue cracks, interface cracks between dissimilar materials, and in joints [1]. Stress singularities take place in linear elastic structures at discontinuities in geometry, material properties, jumps in boundary or interface conditions, and often cause failure initiation due to high stresses [2,3]. Such discontinuities are called singular points (or edges in 3D view) and their neighbourhood as corners, or in general multi-material corners if several materials meet at a singular point. Multi-material corners are present in many kinds of heterogeneous

materials and structural elements, such as composites, multilayers, and polycrystals (e.g., metals, ceramics, rocks, and photovoltaic cells), at different scales, from nanoscale to macroscale. Some of the most relevant publications dealing with theoretical and numerical singularity analysis of isotropic and anisotropic multi-material corners are [4–9] and [10–18], respectively.

As might be expected, frictional contact occurs in many configurations of multi-material corners in deformable structures at different scales, and it is therefore necessary to consider frictional contact in the singularity analysis of such corners for a large number of engineering applications. Although several contact models are available at present, the most commonly used, especially in computational structural analysis, is the Signorini–Coulomb contact model based on the Signorini unilateral contact law and the Coulomb friction law, as it proposes a relatively simple and widely accepted formulation for frictional contact

^{*} Corresponding author.

E-mail address: mantic@us.es (V. Mantič).

problems, [1,19–22]. This is the contact model that will be considered in the following. Due to the inherently non-linear nature of frictional contact, it is more difficult to include such contact in the analysis of singular elastic solutions in multi-material corner problems, than considering only standard linear boundary or interface conditions such as free, clamped, symmetry, etc. Incorporating a true 3D formulation of the Coulomb friction law described by the Coulomb friction cone is particularly difficult.

Thus, although frictional contact has been considered in corner singularity analysis by many authors, they have usually made some simplifying assumptions. In particular, previous works have usually considered linear elastic isotropic materials in contact under plane strain (or plane stress) conditions [1,5,23–30]. Few attempts have been made to analyse corner singularities with frictional contact between anisotropic materials, and even fewer to consider generalised plane strain (GPS) conditions, with the elastic fields independent of the x_3 -coordinate, i.e. $u_i = u_i(x_1, x_2)$ with $i = 1, 2, 3$. In the following, we will focus on the stress singularity analysis of linear elastic anisotropic multi-material corners in GPS with frictional sliding contact.

Several authors simplified the 3D Coulomb friction law, represented by the Coulomb cone, by adopting some simplifying hypotheses. As a result, the collinearity of the frictional tangential stress and relative tangential displacement vectors may not be satisfied in some GPS cases, e.g., with a general orientation of the planes of elastic symmetry (PES) of contacting materials.

For instance, some authors arbitrarily restricted the relative displacement vector (sliding motion vector) in the contact plane to a predetermined direction. In particular, Poonsawat et al. [31] and Magnier et al. [32] simplified the Coulomb frictional contact problem by assuming continuity of displacement in the x_3 -direction between the materials in contact. The differences with respect to the true 3D Coulomb frictional contact model that such a simplification implies in the results of the singularity analysis are discussed in Section 6. A step forward was made by Leguillon [33], who generalised this approach considering any given direction of the relative tangential displacement vector in the contact plane.

In another series of articles, Ting and Chou [34] and Sung and Chung [35] simplified the Coulomb frictional contact law, with the friction coefficient μ , basically assuming that the values of the frictional tangential stresses σ_{12} and σ_{23} are either $\pm\mu\sigma_{22}$ or zero (considering the x_2 -direction normal to the contact x_1x_3 -plane). This assumption may not be valid in configurations where there is no PES coinciding with the $x_3 = 0$ coordinate plane, and where the relative displacements in the x_1 - and x_3 -directions cannot generally be decoupled, leading to incorrect results.

This difficult problem of singularity analysis of linear elastic anisotropic multi-material corners with frictional sliding contact under GPS conditions was solved independently and almost simultaneously in 2012 by Chen et al. [36] and Mantić et al. [37]¹, see also [38], who introduced two new but distinct semi-analytic approaches, both based on the Stroh formalism of anisotropic elasticity [39,40]. The former approach [36] was formulated for a particular case of two anisotropic wedges in a frictional sliding contact, deducing a system of two nonlinear eigenequations for the stress singularity exponent λ and the angle ω of the frictional tangential stress vector measured in the contact plane. The latter approach [37] formulated for multi-material corners with any finite number of faces with isotropic and anisotropic frictional contact, developed an original and general matrix formalism leading to the search for the minimum singular value σ_{\min} of the rectangular matrix of a nonlinear eigenvalue system. σ_{\min} was considered as a function of the stress singularity exponent λ and the angles of the frictional tangential stress vectors ω_w measured in

different contact planes. However, a general and fully operative computational implementation of the latter approach was not developed at that time, only a few preliminary results were presented, so neither any verification by comparison with some previously published results was carried out.

Therefore, the aim of the present article is, first, to thoroughly revise and complete the matrix formalism for the singularity analysis of linear elastic anisotropic multi-material corners with frictional sliding contact under GPS, introduced concisely in [37,38], and secondly, to develop its general computational implementation and to test its performance and accuracy by comparing the obtained results with those available in the relevant literature. This should allow us, in the future, to solve virtually any singularity problem for anisotropic multi-material corners including frictional sliding contact covering any number and type of homogeneous linear elastic materials in each wedge, any type of homogeneous boundary and interface conditions, any geometry of the corner with radial faces.

The present article is in fact a continuation and generalisation of a previous one on the singularity analysis of multi-material linear elastic corners by the present authors [18], where the study was limited to homogeneous (orthogonal) boundary conditions, orthogonal referring to the fact that the stress and displacement vectors are perpendicular to each other, together with interface conditions of perfect bonding or frictionless contact. Here, we focus on the possibility to consider also isotropic frictional sliding contact as boundary or interface condition on any number of faces in the corner. This generalisation requires a substantial modification of the previous matrix formalism developed and implemented in [18], by including additional unknown variables giving angles ω_w of the frictional tangential component of the stress vector and the relative tangential displacement vectors at the faces or interfaces with frictional contact, in view of their collinearity in the isotropic frictional contact. As mentioned above, this modification leads to the solution of a non-linear eigensystem with a rectangular matrix for the singularity exponent λ and angles ω_w . Several numerical procedures are proposed to solve this non-linear eigensystem and their accuracy is tested.

The present semi-analytical matrix formalism is a general mathematical tool capable of solving stress singularity problems under GPS for anisotropic multi-material corners with frictional sliding contact, and with the local geometry near the corner apex and boundary and interface conditions as described in Fig. 1. The study of open or closed (periodic) corners, from the most simple case of single-material and single-wedge case to the multi-material wedge and multi-wedge case of multi-material corners, is covered by this formalism. As in [18], only power singularities are considered, for the sake of simplicity. Thus, special cases of logarithmic or power-logarithmic singularities [4,5,17] are not covered by this formalism, although its semi-analytic nature would allow the study of such singularities if necessary. Theoretically, the geometry of each wedge in the corner is defined by a semi-infinite angular sector.

The article is organised as follows: First, a general analytic expression of a singular elastic solution in a single-material wedge and the transfer matrix are constructed using the Stroh formalism of anisotropic elasticity [39–42] in Section 2. This section is presented in an abridged form, as it was extensively developed in [13,18,37,38]. In Section 3, the matrices for frictional sliding boundary and interface conditions, one of the main novelties of this work, are introduced. The characteristic matrix of the non-linear eigensystem is assembled using the single-material wedge transfer matrices and the boundary and interface condition matrices in Section 4. The implementation of the code is summarised in Section 5, which develops some points for which the reader may need further clarification. The numerical results in Section 6 show perfect agreement with the results for isotropic corners and orthotropic corners, with one PES parallel to the contact plane and another PES perpendicular to the x_3 -axis, found in the literature, but significant differences are sometimes obtained with the results obtained by other authors for orthotropic corners with a general orientation of PES, the reasons for these differences are discussed. Finally, in Section 7 some concluding remarks are given and further developments are proposed.

¹ Book manuscript submitted to the publisher in 2012.

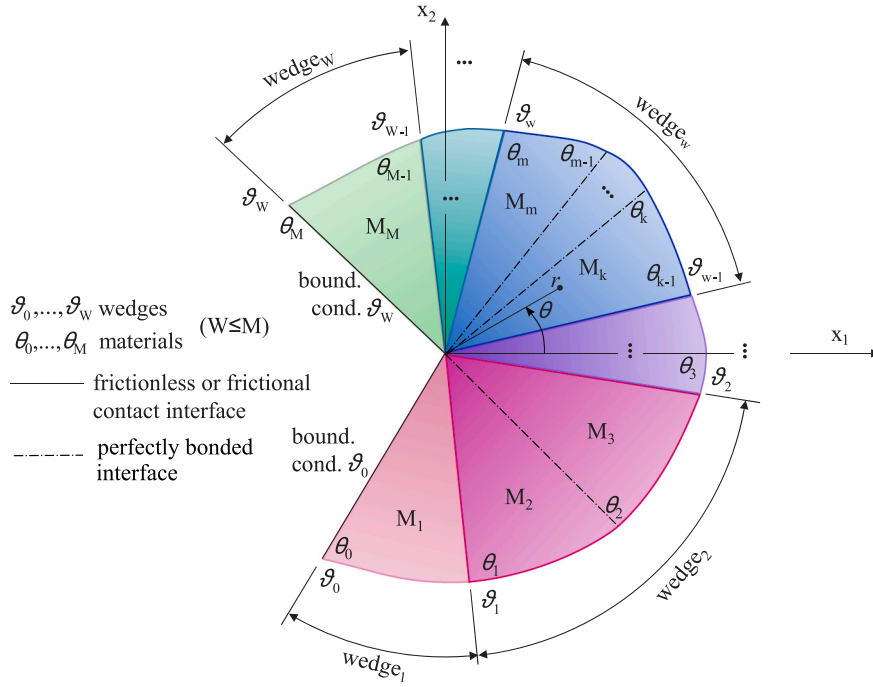


Fig. 1. Schematic of a multi-material corner (2D view).

2. Singular elastic solution for a single-material wedge. Transfer matrix

To describe singular elastic solutions near singular points in linear elastic anisotropic homogeneous materials, the Stroh formalism [39–42] briefly summarised in Appendix A, is used. As mentioned above, in this work, we focus on the power-law singularities, defined by the functions $f_\alpha(z_\alpha) = z_\alpha^\lambda q_\alpha$ (A.13) in the Stroh formalism. Then, the following general expressions can be obtained for the power-law displacement and stress function vectors, as shown in Appendix A,

$$\mathbf{u} = r^\lambda \{ \mathbf{A} \langle \zeta_*^\lambda \rangle \mathbf{q} + \bar{\mathbf{A}} \langle \bar{\zeta}_*^\lambda \rangle \bar{\mathbf{q}} \}, \quad (1)$$

$$\boldsymbol{\varphi} = r^\lambda \{ \mathbf{B} \langle \zeta_*^\lambda \rangle \mathbf{q} + \bar{\mathbf{B}} \langle \bar{\zeta}_*^\lambda \rangle \bar{\mathbf{q}} \}, \quad (2)$$

where \mathbf{A} and \mathbf{B} are 3×3 complex square matrices that depend on the elastic properties of the material defined in (A.17), \mathbf{q} and $\bar{\mathbf{q}}$ are arbitrary constant vectors, $\langle \zeta_*^\lambda \rangle$ is a diagonal matrix defined in (A.16), and the overbar denotes complex conjugate matrix. These expressions can be arranged in a more compact form by defining the 6×1 vector of elastic variables $\mathbf{w}(r, \theta)$ in (A.18).

2.1. Transfer matrix

This section briefly presents the very useful transfer matrix concept introduced by Ting [10], see [13,37,38] for a more detailed analysis. The transfer matrix for the single-material wedge of number m , $\mathbf{E}_m(\lambda, \theta_m, \theta_{m-1})$, gives a relation between the power-law solution values on the two faces of the wedge, $\mathbf{w}_m(r, \theta_{m-1})$ and $\mathbf{w}_m(r, \theta_m)$, see Fig. 2,

$$\mathbf{w}_m(r, \theta_m) = \mathbf{E}_m(\lambda, \theta_m, \theta_{m-1}) \mathbf{w}_m(r, \theta_{m-1}). \quad (3)$$

The transfer matrix for a given λ depends on the properties of the wedge material and the wedge geometry as

$$\mathbf{E}_m(\lambda, \theta_m, \theta_{m-1}) = \mathbf{X} \mathbf{Z}^\lambda(\theta_m, \theta_{m-1}) \mathbf{X}^{-1}, \quad (4)$$

where \mathbf{X} is defined in (A.19), and

$$\mathbf{Z}^\lambda(\theta_m, \theta_{m-1}) = \begin{bmatrix} \langle \zeta_*^\lambda(\theta_m, \theta_{m-1}) \rangle & 0 \\ 0 & \langle \bar{\zeta}_*^\lambda(\theta_m, \theta_{m-1}) \rangle \end{bmatrix}, \quad (5)$$

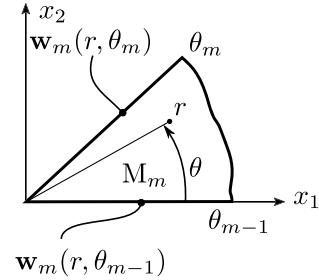


Fig. 2. Schema of a single-material wedge.

with

$$\langle \zeta_*^\lambda(\theta_m, \theta_{m-1}) \rangle = \text{diag} (\zeta_1^\lambda(\theta_m, \theta_{m-1}), \zeta_2^\lambda(\theta_m, \theta_{m-1}), \zeta_3^\lambda(\theta_m, \theta_{m-1})), \quad (6)$$

$$\langle \bar{\zeta}_*^\lambda(\theta_m, \theta_{m-1}) \rangle = \text{diag} (\bar{\zeta}_1^\lambda(\theta_m, \theta_{m-1}), \bar{\zeta}_2^\lambda(\theta_m, \theta_{m-1}), \bar{\zeta}_3^\lambda(\theta_m, \theta_{m-1})), \quad (7)$$

$$\zeta_\alpha(\theta_m, \theta_{m-1}) = \cos(\theta_m - \theta_{m-1}) + p_\alpha(\theta_{m-1}) \sin(\theta_m - \theta_{m-1}), \quad (7)$$

and

$$p_\alpha(\theta_{m-1}) = \frac{p_\alpha \cos(\theta_{m-1}) - \sin(\theta_{m-1})}{p_\alpha \sin(\theta_{m-1}) + \cos(\theta_{m-1})}. \quad (8)$$

Regarding the computational implementation of the complex power functions in (6) keeping their continuity, see a detailed discussion in [18].

3. Matrix formalism for boundary and interface conditions

3.1. Reference frame attached to a corner face

A basis of orthonormal vectors attached to a face of the multi-material corner, see Fig. 3 and [18, Fig. 2],

$$(\mathbf{s}_r(\vartheta), \mathbf{s}_3, \mathbf{n}(\vartheta)), \quad (9)$$

with the vectors expressed in the Cartesian coordinates as

$$\mathbf{s}_r(\vartheta) = \begin{pmatrix} -\cos(\vartheta) \\ -\sin(\vartheta) \\ 0 \end{pmatrix}, \quad \mathbf{s}_3 = \begin{pmatrix} 0 \\ 0 \\ 1 \end{pmatrix}, \quad \mathbf{n}(\vartheta) = \begin{pmatrix} -\sin(\vartheta) \\ \cos(\vartheta) \\ 0 \end{pmatrix}, \quad (10)$$

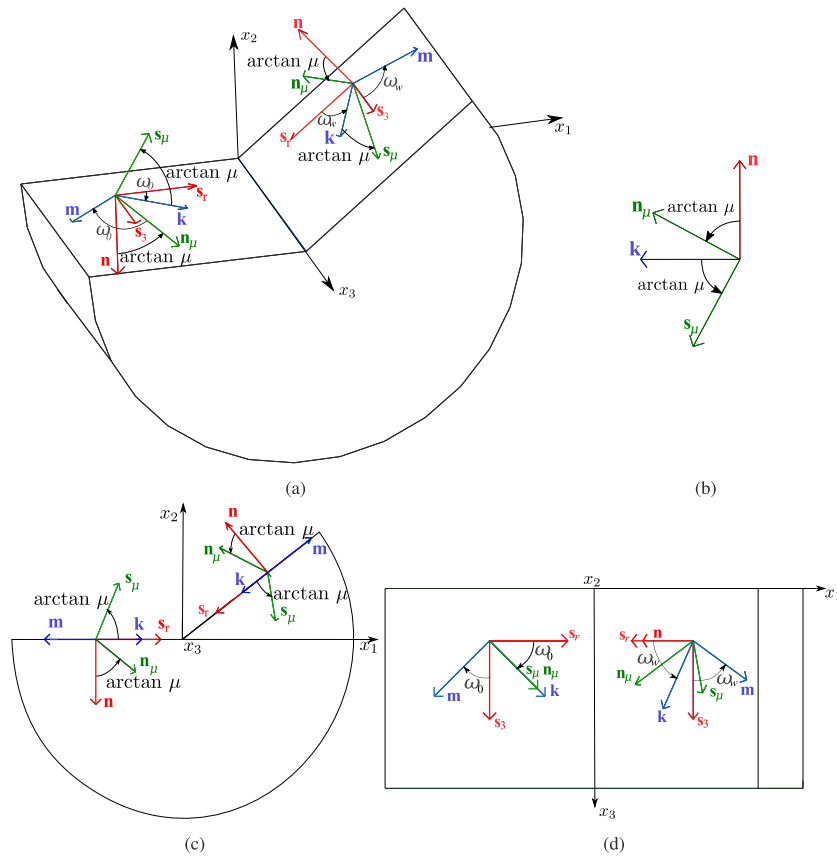


Fig. 3. Orthonormal bases attached to each face of a multi-material corner for frictional sliding contact. (a) 3D view of an open corner with orthonormal basis on its outer faces, (b) vectors in the plane defined by \mathbf{k} and \mathbf{n} , (c) orthogonal projection on the x_1x_2 -plane, (d) orthogonal projection on the x_1x_3 -plane.

defines a useful reference frame for the displacement and traction vectors. The angle ϑ in (10) is defined in Fig. 1.

To describe the isotropic frictional sliding contact within the framework of the present matrix formalism, it is first necessary to define two orthonormal bases for the sliding and frictional shear stress directions, which make it easy to impose the necessary conditions, see Fig. 3,

$$(\mathbf{k}(\vartheta, \omega), \mathbf{m}(\vartheta, \omega), \mathbf{n}(\vartheta)) \tag{11}$$

$$(\mathbf{n}_\mu(\vartheta, \omega, \mu), \mathbf{s}_\mu(\vartheta, \omega, \mu), \mathbf{m}(\vartheta, \omega)), \tag{12}$$

with

$$\mathbf{k}(\vartheta, \omega) = \cos(\omega)\mathbf{s}_r(\vartheta) + \sin(\omega)\mathbf{s}_3, \tag{13}$$

$$\mathbf{m}(\vartheta, \omega) = -\sin(\omega)\mathbf{s}_r(\vartheta) + \cos(\omega)\mathbf{s}_3, \tag{14}$$

$$\mathbf{n}_\mu(\vartheta, \omega, \mu) = \frac{\mathbf{n}(\vartheta) + \mu\mathbf{k}(\vartheta, \omega)}{\sqrt{1 + \mu^2}}, \tag{15}$$

$$\mathbf{s}_\mu(\vartheta, \omega, \mu) = \frac{\mathbf{k}(\vartheta, \omega) - \mu\mathbf{n}(\vartheta)}{\sqrt{1 + \mu^2}}, \tag{16}$$

where $\mu \geq 0$ is a given constant value of the kinetic (or dynamic) friction coefficient on the face of the wedge, and the unknown value of the angle ω gives the direction of the tangential component $\boldsymbol{\tau}$ of the stress vector² \mathbf{t} associated with the normal vector $\mathbf{n}(\vartheta)$, on the face at the angle ϑ , in the sense that

$$\boldsymbol{\tau} = -|\boldsymbol{\tau}|\mathbf{k}(\vartheta, \omega), \tag{17}$$

Therefore, the unit vector $\mathbf{k}(\vartheta, \omega)$ determines the direction of the tangential stress vector $\boldsymbol{\tau}$. Vectors \mathbf{n}_μ and \mathbf{s}_μ are used in Sections 3.3 and 3.4 and the reason for choosing these vectors is explained in Appendices B and C.

The subscript w has been omitted in the above vector definitions, for the sake of simplicity, but each wedge face in a multi-material corner under friction can have a different value of μ and ω .

3.2. Signorini-Coulomb conditions for frictional sliding contact on a boundary

The frictional contact model adopted in the present work is the well-known Amontons–Coulomb friction model (or simply the Coulomb model). For frictional sliding contact as a boundary condition for the face number $w = 0$ or W , a null displacement must be imposed in the normal direction to the face.

$$u_\theta(r, \vartheta_w) = 0. \tag{18}$$

In this work, only $\mu \geq 0$ is considered, since a negative value of the friction coefficient considered by some other authors [23,26,29,31] corresponds in the present formulation with a sliding direction in the opposite sense to that obtained with a positive friction coefficient, that is, with angles $\omega \pm 180^\circ$ and ω , respectively. The shear stress vector $\boldsymbol{\tau}(r, \vartheta_w)$ and the normal stress $\sigma_{\theta\theta}(r, \vartheta_w)$ are related by the Coulomb friction coefficient μ

$$|\boldsymbol{\tau}(r, \vartheta_w)| = -\mu\sigma_{\theta\theta}(r, \vartheta_w), \tag{19}$$

where the shear stress vector on the faces with the number $w = 0$ or W is

$$\boldsymbol{\tau}(r, \vartheta_w) = -\sigma_{\theta r}\mathbf{s}_r(\vartheta_w) + \sigma_{\theta 3}(r, \vartheta_w)\mathbf{s}_3. \tag{20}$$

² Usually referred to as the tangential stress vector.

Table 1
Matrices \mathbf{D}_u and \mathbf{D}_φ for Coulomb sliding friction.

$\mathbf{D}_u(\vartheta, \omega) = [\mathbf{n}(\vartheta), \mathbf{0}, \mathbf{m}(\vartheta, \omega), \mathbf{0}]^T$	$\mathbf{D}_\varphi(\vartheta, \omega, \mu) = [\mathbf{0}, s_r(\vartheta, \omega, \mu), \mathbf{0}, \mathbf{m}(\vartheta, \omega)]^T$
$\tilde{\mathbf{D}}_u(\vartheta, \omega) = [\mathbf{0}, \mathbf{k}(\vartheta, \omega)]^T$	$\tilde{\mathbf{D}}_\varphi(\vartheta, \omega, \mu) = [\mathbf{n}_\mu(\vartheta, \omega, \mu), \mathbf{0}]^T$

The last condition for frictional sliding contact is that the (tangential) displacement vector, $\mathbf{u}^i(r, \vartheta_w)$, and the tangential stress vector $\boldsymbol{\tau}^i(r, \vartheta_w)$ must be parallel, i denoting the wedge number and w denoting the face number,

$$\boldsymbol{\tau}^i(r, \vartheta_w) = -\kappa \mathbf{u}^i(r, \vartheta_w) \quad \text{with} \quad \begin{cases} \kappa \leq 0 & \text{for } i = 1 \text{ and } w = 0 \\ \kappa \geq 0 & \text{for } i = W \text{ and } w = W \end{cases} \quad (21)$$

choosing the sign of κ so that the direction of the physical tangential stress is opposite to the direction of sliding to satisfy the condition of frictional dissipation of energy.

In Appendix B, these contact conditions are related to the reference frames presented in Section 3.1 for a better comprehension of the matrices presented in Section 3.3. The non-linear frictionless or frictional sliding contact conditions are first imposed as linear boundary or interface conditions, which is one of the main ideas behind this formalism. Then, after solving the corner eigenproblem, each obtained eigensolution is checked for the fulfilment of the compression condition on all contact surfaces, and for the frictional energy dissipation condition. Only eigensolutions verifying these non-linear conditions are valid.

3.3. Boundary condition matrices for frictional contact

As the traction vector at a point of a wedge face, associated to the normal vector \mathbf{n} defined in (10), can be calculated as

$$\mathbf{t}^n(x_1, x_2) = -\frac{\partial \boldsymbol{\varphi}}{\partial s_r}(x_1, x_2) = \frac{\partial \boldsymbol{\varphi}}{\partial r}, \quad (22)$$

both vectors \mathbf{t}^n and $\boldsymbol{\varphi}$ are parallel, in view of (2), and we can consider a zero stress function vector $\boldsymbol{\varphi}$ at the edge of the wedge ($r = 0$), i.e. the wedge apex in 2D view. Then, the usual homogeneous (orthogonal) boundary conditions for $r > 0$ at faces $w = 0$ and $w = W$ can be expressed as a linear relation

$$\mathbf{D}_u(\vartheta_w) \mathbf{u}(r, \vartheta_w) + \mathbf{D}_\varphi(\vartheta_w) \boldsymbol{\varphi}(r, \vartheta_w) = \mathbf{0}, \quad (23)$$

where $\mathbf{D}_u(\vartheta_w)$ and $\mathbf{D}_\varphi(\vartheta_w)$ are 3×3 real matrices presented in [18, Table 1] that fulfil the orthogonality relations shown in [13,18,37,38,43].

The frictional contact boundary conditions described in Section 3.2 are imposed by using suitable boundary condition matrices defined in the following. In contrast to the boundary conditions in [18, Table 1], the matrices \mathbf{D}_u and \mathbf{D}_φ for the frictional contact boundary condition introduced in Table 1 are non-square real matrices and do not fulfil the same orthogonality relation. These matrices are rectangular, having one row more than the matrices for orthogonal boundary conditions. This extra row leads to four boundary conditions instead of three. This additional boundary condition is associated with the fact that a certain direction of shear component of the traction vector ω is assumed here, although, in general, the value of ω is unknown a priori and is computed by solving the corner eigenvalue problem.

To express the boundary conditions of frictional contact, for boundary faces $w = 0$ and W , as a linear relation in a way similar to that in (23)

$$\mathbf{D}_u(\vartheta_w, \omega_w) \mathbf{u}(r, \vartheta_w) + \mathbf{D}_\varphi(\vartheta_w, \omega_w, \mu_w) \boldsymbol{\varphi}(r, \vartheta_w) = \mathbf{0}, \quad (24)$$

the following hypothesis must be assumed: the whole face is sliding in the same direction, with ω and μ constant on the whole face, and a monotonic loading is applied from the unloaded state. In this way, the non-linearities associated with the unilateral Signorini conditions of non-penetration and the Coulomb friction law are avoided.

For the homogeneous (orthogonal) boundary condition (23), the main boundary-condition-matrix, \mathbf{D}_{BC} is expressed as, see [18, Table 1],

$$\mathbf{D}_{BC}(\vartheta_w) = \begin{bmatrix} \mathbf{D}_u(\vartheta_w) & \mathbf{D}_\varphi(\vartheta_w) \\ \tilde{\mathbf{D}}_u(\vartheta_w) & \tilde{\mathbf{D}}_\varphi(\vartheta_w) \end{bmatrix} = \begin{bmatrix} \mathbf{D}_u(\vartheta_w) & \mathbf{D}_\varphi(\vartheta_w) \\ \mathbf{D}_\varphi(\vartheta_w) & \mathbf{D}_u(\vartheta_w) \end{bmatrix}, \quad (25)$$

whereas for the frictional sliding condition matrices in (24) as, see Table 1,

$$\mathbf{D}_{BC}(\vartheta_w, \omega_w, \mu_w) = \begin{bmatrix} \mathbf{D}_u(\vartheta_w, \omega_w) & \mathbf{D}_\varphi(\vartheta_w, \omega_w, \mu_w) \\ \tilde{\mathbf{D}}_u(\vartheta_w, \omega_w) & \tilde{\mathbf{D}}_\varphi(\vartheta_w, \omega_w, \mu_w) \end{bmatrix}. \quad (26)$$

Similarly, as discussed in [18], in the frictional contact case, the matrices in Table 1 are not uniquely defined. It is easy to show that the matrix \mathbf{D}_{BC} is a real square matrix 6×6 that fulfils the orthogonality relation, cf. [13,18,37,38,43],

$$\mathbf{D}_{BC} \mathbf{D}_{BC}^T = \mathbf{D}_{BC}^T \mathbf{D}_{BC} = \mathbf{I}_{6 \times 6}. \quad (27)$$

The orthogonality relation in (27) is equivalent to the following relations for the matrices in Table 1:

$$\mathbf{D}_u \mathbf{D}_u^T + \mathbf{D}_\varphi \mathbf{D}_\varphi^T = \mathbf{I}_{4 \times 4}, \quad (28)$$

$$\mathbf{D}_u \tilde{\mathbf{D}}_u^T + \mathbf{D}_\varphi \tilde{\mathbf{D}}_\varphi^T = \mathbf{0}_{4 \times 2}, \quad (29)$$

$$\tilde{\mathbf{D}}_u \mathbf{D}_u^T + \tilde{\mathbf{D}}_\varphi \mathbf{D}_\varphi^T = \mathbf{0}_{2 \times 4}, \quad (30)$$

$$\tilde{\mathbf{D}}_u \tilde{\mathbf{D}}_u^T + \tilde{\mathbf{D}}_\varphi \tilde{\mathbf{D}}_\varphi^T = \mathbf{I}_{2 \times 2}. \quad (31)$$

When multiplying from the left the vector $\mathbf{w}(r, \vartheta_w)$ by the matrix \mathbf{D}_{BC} in (25) or (26), the prescribed and unknown components of $\mathbf{w}(r, \vartheta_w)$ appear grouped in two separate blocks, $\mathbf{w}_p(r, \vartheta_w)$ and $\mathbf{w}_U(r, \vartheta_w)$, respectively,

$$\mathbf{D}_{BC} \mathbf{w}(r, \vartheta_w) = \begin{bmatrix} \mathbf{w}_p(r, \vartheta_w) \\ \mathbf{w}_U(r, \vartheta_w) \end{bmatrix}. \quad (32)$$

The vectors \mathbf{w}_p and \mathbf{w}_U are 3×1 vectors for the homogeneous (orthogonal) boundary conditions in [18, Table 1], but, in case of frictional sliding contact, \mathbf{w}_p is a 4×1 vector and \mathbf{w}_U is a 2×1 vector. Taking into account the orthogonality relation in (27) and the fact that $\mathbf{w}_p = \mathbf{0}$,

$$\mathbf{w}(r, \vartheta_w) = \mathbf{D}_{BC}^T \begin{bmatrix} \mathbf{w}_p(r, \vartheta_w) \\ \mathbf{w}_U(r, \vartheta_w) \end{bmatrix} = \begin{bmatrix} \tilde{\mathbf{D}}_u^T \\ \tilde{\mathbf{D}}_\varphi^T \end{bmatrix} \mathbf{w}_U(r, \vartheta_w) = \tilde{\mathbf{D}}_{BC}^T \mathbf{w}_U(r, \vartheta_w) \quad (33)$$

for $w = 0$ and W .

3.4. Signorini-Coulomb conditions for frictional sliding contact on an interface

For frictional sliding contact as an interface condition for faces at angle ϑ_w , with $1 \leq w \leq W - 1$, for open corners, and $0 \leq w \leq W$ for closed (periodic) corners, a null relative normal displacement must be imposed between the two wedges in contact;

$$\Delta u_\theta(r, \vartheta_w) = u_\theta^w(r, \vartheta_w) - u_\theta^{w+1}(r, \vartheta_w) = 0. \quad (34)$$

The tangential stress vector $\boldsymbol{\tau}(r, \vartheta_w)$ (20) and the normal stress are related by the Coulomb friction coefficient μ as in (19). Additionally, a continuity condition of tractions (in fact an equilibrium of tractions) must be imposed for the materials in contact,

$$\mathbf{t}^w(\vartheta_w) - \mathbf{t}^{w+1}(\vartheta_w) = \mathbf{0}. \quad (35)$$

At the interface, the relative tangential displacement vector is defined as

$$\Delta \mathbf{u}(r, \vartheta_w) = -\Delta u_r(r, \vartheta_w) \mathbf{s}_r(r, \vartheta_w) + \Delta u_3(r, \vartheta_w) \mathbf{s}_3(r, \vartheta_w), \quad (36)$$

where

$$\begin{aligned} \Delta u_r(r, \vartheta_w) &= u_r^w(r, \vartheta_w) - u_r^{w+1}(r, \vartheta_w), \\ \Delta u_3(r, \vartheta_w) &= u_3^w(r, \vartheta_w) - u_3^{w+1}(r, \vartheta_w). \end{aligned} \quad (37)$$

Table 2
Matrices \mathbf{D}_1 , \mathbf{D}_2 , $\tilde{\mathbf{D}}_1$ and $\tilde{\mathbf{D}}_2$ for frictional interface contact conditions.

Frictional interface	$\mathbf{D}_1(\vartheta, \omega, \mu) = \frac{1}{\sqrt{2}} \begin{bmatrix} -\mathbf{n}(\vartheta) & \mathbf{0}_{3 \times 1} & \mathbf{0}_{3 \times 3} & -\mathbf{m}(\vartheta, \omega) & \mathbf{0}_{3 \times 1} \\ \mathbf{0}_{3 \times 1} & s_\mu(\vartheta, \omega, \mu) & -\mathbf{I}_{3 \times 3} & \mathbf{0}_{3 \times 1} & \mathbf{m}(\vartheta, \omega) \end{bmatrix}^T$
	$\mathbf{D}_2(\vartheta, \omega, \mu) = \frac{1}{\sqrt{2}} \begin{bmatrix} \mathbf{n}(\vartheta) & \mathbf{0}_{3 \times 1} & \mathbf{0}_{3 \times 3} & \mathbf{m}(\vartheta, \omega) & \mathbf{0}_{3 \times 1} \\ \mathbf{0}_{3 \times 1} & s_\mu(\vartheta, \omega, \mu) & \mathbf{I}_{3 \times 3} & \mathbf{0}_{3 \times 1} & \mathbf{m}(\vartheta, \omega) \end{bmatrix}^T$
	$\tilde{\mathbf{D}}_1(\vartheta, \omega, \mu) = \frac{1}{\sqrt{2}} \begin{bmatrix} \mathbf{n}(\vartheta) & \mathbf{0}_{3 \times 1} & \sqrt{2}\mathbf{k}(\vartheta, \omega) & \mathbf{0}_{3 \times 1} & \mathbf{m}(\vartheta, \omega) \\ \mathbf{0}_{3 \times 1} & \mathbf{n}_\mu(\vartheta, \omega, \mu) & \mathbf{0}_{3 \times 1} & \mathbf{0}_{3 \times 1} & \mathbf{0}_{3 \times 1} \end{bmatrix}^T$
	$\tilde{\mathbf{D}}_2(\vartheta, \omega, \mu) = \frac{1}{\sqrt{2}} \begin{bmatrix} \mathbf{n}(\vartheta) & \mathbf{0}_{3 \times 1} & \mathbf{0}_{3 \times 1} & \sqrt{2}\mathbf{k}(\vartheta, \omega) & \mathbf{m}(\vartheta, \omega) \\ \mathbf{0}_{3 \times 1} & \mathbf{n}_\mu(\vartheta, \omega, \mu) & \mathbf{0}_{3 \times 1} & \mathbf{0}_{3 \times 1} & \mathbf{0}_{3 \times 1} \end{bmatrix}^T$

To satisfy the condition of frictional dissipation of energy, the tangential stress vector $\boldsymbol{\tau}^i$, acting on the face of the wedge $i = w, w + 1$, must be parallel to $\Delta \mathbf{u}(r, \vartheta_w)$ but with the opposite direction. Therefore,

$$\boldsymbol{\tau}^i = -\kappa \Delta \mathbf{u}(r, \vartheta_w) \quad \text{with } \kappa \geq 0, \quad (38)$$

or component-wise

$$\begin{aligned} \tau_r^i(r, \vartheta_w) &= \sigma_{\theta_r}^i(r, \vartheta_w) = -\kappa (u_r^w(r, \vartheta_w) - u_r^{w+1}(r, \vartheta_w)), \\ \tau_3^i(r, \vartheta_w) &= \sigma_{\theta_3}^i(r, \vartheta_w) = -\kappa (u_3^w(r, \vartheta_w) - u_3^{w+1}(r, \vartheta_w)). \end{aligned} \quad (39)$$

In Appendix C, these contact conditions are related to the reference frames presented in Section 3.1 for a better comprehension of the matrices presented in Section 3.5.

3.5. Interface condition matrices for frictional contact

For a perfectly bonded interface or for a frictionless sliding interface, the following linear condition must be satisfied for the matrices introduced in [18, Table 2], similar to (23) for the homogeneous boundary condition,

$$\mathbf{D}_1(\vartheta_w) \mathbf{w}_w(r, \vartheta_w) + \mathbf{D}_2(\vartheta_w) \mathbf{w}_{w+1}(r, \vartheta_w) = \mathbf{0}, \quad (40)$$

These matrices also satisfy the orthogonality relation presented in [18, 37, 38].

The frictional contact interface conditions described in Section 3.4 are imposed by using suitable interface condition matrices defined in the following. Similarly to the frictional sliding boundary condition, in the case of the frictional sliding contact interface condition, a certain friction shear direction (or sliding direction) given by the angle ω is assumed here, which means that there are seven interface conditions instead of the expected six conditions. Therefore, the matrices \mathbf{D}_1 and \mathbf{D}_2 , presented in Table 2, are rectangular 7×6 real matrices, while $\tilde{\mathbf{D}}_1$ and $\tilde{\mathbf{D}}_2$ are rectangular 5×6 real matrices. As in the previous section, the expressions of these matrices in Table 2 are just a convenient example of possible options to impose the frictional interface contact.

To express the frictional contact interface condition as a linear relation for vectors of elastic variables, the same hypothesis as adopted in the previous section for the friction boundary condition must be applied, leading to

$$\mathbf{D}_1(\vartheta_w, \omega_w, \mu_w) \mathbf{w}_w(r, \vartheta_w) + \mathbf{D}_2(\vartheta_w, \omega_w, \mu_w) \mathbf{w}_{w+1}(r, \vartheta_w) = \mathbf{0}. \quad (41)$$

The *main interface-condition matrix* defined for the interface frictional contact condition is a 12×12 real matrix \mathbf{D}_I , analogous to the matrix \mathbf{D}_{BC} for boundary conditions. For perfectly bonded interface and frictionless sliding condition, this matrix is defined as

$$\mathbf{D}_I(\vartheta_w) = \begin{bmatrix} \mathbf{D}_1(\vartheta_w) & \mathbf{D}_2(\vartheta_w) \\ \tilde{\mathbf{D}}_1(\vartheta_w) & \tilde{\mathbf{D}}_2(\vartheta_w) \end{bmatrix}, \quad (42)$$

whereas for the frictional contact interface as

$$\mathbf{D}_I(\vartheta_w, \omega_w, \mu_w) = \begin{bmatrix} \mathbf{D}_1(\vartheta_w, \omega_w, \mu_w) & \mathbf{D}_2(\vartheta_w, \omega_w, \mu_w) \\ \tilde{\mathbf{D}}_1(\vartheta_w, \omega_w, \mu_w) & \tilde{\mathbf{D}}_2(\vartheta_w, \omega_w, \mu_w) \end{bmatrix}. \quad (43)$$

Again, it can easily be checked that the matrix \mathbf{D}_I in (43) fulfils the orthogonality relation

$$\mathbf{D}_I \mathbf{D}_I^T = \mathbf{D}_I^T \mathbf{D}_I = \mathbf{I}_{12 \times 12}. \quad (44)$$

This orthogonality relation is analogous to the orthogonality relations for a perfectly bonded interface and a frictionless sliding interface deduced in [18, Eq. (50)], and is equivalent to the following relations for the matrices in Table 2 for the frictional sliding interface

$$\begin{aligned} \mathbf{D}_1 \mathbf{D}_1^T + \mathbf{D}_2 \mathbf{D}_2^T &= \mathbf{I}_{7 \times 7}, \\ \mathbf{D}_1 \tilde{\mathbf{D}}_1^T + \mathbf{D}_2 \tilde{\mathbf{D}}_2^T &= \mathbf{0}_{7 \times 5}, \\ \tilde{\mathbf{D}}_1 \mathbf{D}_1^T + \tilde{\mathbf{D}}_2 \mathbf{D}_2^T &= \mathbf{0}_{5 \times 7}, \\ \tilde{\mathbf{D}}_1 \tilde{\mathbf{D}}_1^T + \tilde{\mathbf{D}}_2 \tilde{\mathbf{D}}_2^T &= \mathbf{I}_{5 \times 5}. \end{aligned} \quad (45)$$

Multiplying a 12×1 vector given by two 6×1 vectors $\mathbf{w}(r, \vartheta)$ defined on the face w of the two consecutive wedges, w and $w + 1$, from the left by the matrix \mathbf{D}_I , the vectors $\mathbf{w}_p(r, \vartheta)$ and $\mathbf{w}_U(r, \vartheta)$ of the prescribed and unknown elastic variables, respectively, are obtained

$$\mathbf{D}_I \begin{bmatrix} \mathbf{w}_w(r, \vartheta_w) \\ \mathbf{w}_{w+1}(r, \vartheta_w) \end{bmatrix} = \begin{bmatrix} \mathbf{w}_p(r, \vartheta_w) \\ \mathbf{w}_U(r, \vartheta_w) \end{bmatrix}, \quad (46)$$

where \mathbf{w}_p is a 7×1 vector and \mathbf{w}_U is a 5×1 vector. Then, by multiplying (46) from the left by \mathbf{D}_I^T , using the orthogonality relation (44) and taking into account that $\mathbf{w}_p = \mathbf{0}$ we get a very relevant expression of the interface elastic variables in terms of \mathbf{w}_U ,

$$\begin{bmatrix} \mathbf{w}_w(r, \vartheta_w) \\ \mathbf{w}_{w+1}(r, \vartheta_w) \end{bmatrix} = \mathbf{D}_I^T \begin{bmatrix} \mathbf{w}_p(r, \vartheta_w) \\ \mathbf{w}_U(r, \vartheta_w) \end{bmatrix} = \begin{bmatrix} \tilde{\mathbf{D}}_1^T \\ \tilde{\mathbf{D}}_2^T \end{bmatrix} \mathbf{w}_U(r, \vartheta_w). \quad (47)$$

Once the characteristic system for the corner singularity analysis described in the next section is solved, the fulfilment of the compression condition must be checked, for both frictionless and frictional sliding contacts. Furthermore, for frictional sliding contact, the conditions for frictional dissipation of energy (21) and (38) should be checked.

4. Characteristic system for the stress singularity analysis in a multi-material elastic corner with frictional contact

Up to this point, the analysis has focused on a single-material wedge and a boundary or interface condition. In this section, first, all material transfer matrices are used to define the *multi-material wedge transfer matrix*, and the *extended matrix of transfer relations of the multi-material corner*. Moreover, all the boundary and interface matrices of the corner are used to assembly the *extended boundary and interface condition matrix of the multi-material corner*. With these two matrices and the vector of elastic variables at the corner, the *characteristic system of the corner* is constructed.

4.1. Multi-material wedge transfer matrix

A multi-material wedge w is defined by two or more perfectly bonded single-material wedges with consecutive indices $i_w, i_w + 1, \dots, j_w - 1, j_w$, where i_w and j_w are the indices of the first and last material in the wedge w . The procedure to construct its *multi-material wedge transfer matrix*, explained in detail in [18, Section 5.1], can also be applied here, leading to the multiplication of all successive *single-material wedge transfer matrices* in the wedge (4) as follows

$$\mathbf{K}_w(\lambda) = \mathbf{E}_{j_w}(\lambda) \cdot \mathbf{E}_{j_w-1}(\lambda) \dots \mathbf{E}_{i_w+1}(\lambda) \cdot \mathbf{E}_{i_w}(\lambda). \quad (48)$$

The size of the final characteristic system of the corner to be solved may be significantly reduced by using this matrix for each multi-material wedge in the corner; see [18, Section 5].

The assembly of the characteristic system of a multi-material corner is based on the *transfer relation for a multi-material wedge* w defined as

$$[\mathbf{K}_w(\lambda) - \mathbf{I}_{6 \times 6}] \begin{bmatrix} \mathbf{w}_w(r, \vartheta_{w-1}) \\ \mathbf{w}_w(r, \vartheta_w) \end{bmatrix} = \mathbf{0}_{6 \times 1}. \quad (49)$$

4.2. Characteristic system assembly for a multi-material corner

When a corner consists of two or more multi-material wedges, the corresponding multi-material wedge transfer matrices are collected in the $6W \times 12W$ *extended matrix of transfer relations of the multi-material corner*

$$\mathbf{K}_{\text{corner_ext.}}(\lambda) = \begin{bmatrix} \mathbf{K}_1(\lambda) & -\mathbf{I}_{6 \times 6} & \mathbf{0}_{6 \times 6} & \mathbf{0}_{6 \times 6} & \cdots & \cdots & \mathbf{0}_{6 \times 6} \\ \mathbf{0}_{6 \times 6} & \mathbf{0}_{6 \times 6} & \mathbf{K}_2(\lambda) & -\mathbf{I}_{6 \times 6} & \cdots & \cdots & \mathbf{0}_{6 \times 6} \\ \vdots & \vdots & \vdots & \vdots & \ddots & \vdots & \vdots \\ \mathbf{0}_{6 \times 6} & \mathbf{0}_{6 \times 6} & \mathbf{0}_{6 \times 6} & \mathbf{0}_{6 \times 6} & \cdots & \mathbf{K}_W(\lambda) & -\mathbf{I}_{6 \times 6} \end{bmatrix}. \quad (50)$$

This matrix depends not only on λ , but also on the properties of the materials and the polar sector angles of all single-material wedges in the corner. In the case that we are dealing with corners with two or more multi-material or single-material wedges, the vector given by the displacement and stress function vectors at outer faces and interfaces has the following form

$$\mathbf{w}_{\text{corner_ext.}} = \begin{bmatrix} \mathbf{w}_1(r, \vartheta_0) \\ \mathbf{w}_1(r, \vartheta_1) \\ \mathbf{w}_2(r, \vartheta_1) \\ \mathbf{w}_2(r, \vartheta_2) \\ \vdots \\ \mathbf{w}_W(r, \vartheta_{W-1}) \\ \mathbf{w}_W(r, \vartheta_W) \end{bmatrix}. \quad (51)$$

All transfer relations (49) for multi-material wedges in the corner can be written in a compact form as

$$\mathbf{K}_{\text{corner_ext.}}(\lambda) \mathbf{w}_{\text{corner_ext.}} = \mathbf{0}_{6W \times 1}. \quad (52)$$

In the following subsections, a new extended boundary and interface condition matrix $\mathbf{D}_{\text{corner_ext}}$ is constructed using the boundary and interface condition matrices, for open corners in (57) and for closed corners in (65). As the matrices \mathbf{D}_{BC} and \mathbf{D}_{I} , respectively, satisfy the orthogonality relation in (27) and (44), the matrix $\mathbf{D}_{\text{corner_ext}}$ satisfies the orthogonality relation

$$\mathbf{D}_{\text{corner_ext}}(\vartheta, \omega, \mu) \mathbf{D}_{\text{corner_ext}}^T(\vartheta, \omega, \mu) = \mathbf{I}_{12W \times 12W}, \quad (53)$$

where

$$\vartheta = (\vartheta_0, \vartheta_1, \dots, \vartheta_W), \quad (54)$$

is the vector of polar angles of multi-material wedge faces in the corner. The vectors of the unknown values of the angle of friction shear stress vector and the values of friction coefficient on the boundary faces and interfaces with frictional contact are defined as

$$\omega = (\omega_{k_1}, \omega_{k_2}, \dots, \omega_{k_{F-1}}, \omega_{k_F}) \quad (55)$$

and

$$\mu = (\mu_{k_1}, \mu_{k_2}, \dots, \mu_{k_{F-1}}, \mu_{k_F}). \quad (56)$$

The set of F sub-indices k_i ($i = 1, \dots, F$), $0 \leq k_1 < k_2 < \dots < k_{F-1} < k_F \leq W$ ($0 \leq F \leq W + 1$), in (55) and (56), is defined by the numbers of boundary faces or interfaces with frictional sliding contact. There are F faces of this type in the corner. An illustration of this group of indices is shown in Fig. 4, where a corner made up of 6 wedges is depicted, with 3 and 4 faces, respectively, with frictionless and frictional contact.

If there is no frictional boundary or interface condition, $F = 0$, and ω and μ are not defined, and the corner problem reduces to that analysed in [18].

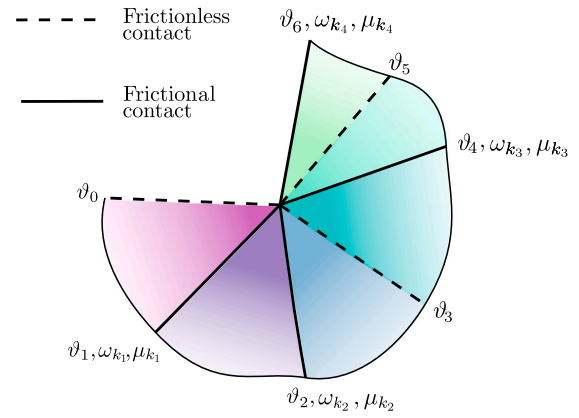


Fig. 4. Schema of a corner with frictionless and frictional boundary and interface conditions.

4.2.1. Open corner

Open corners have two outer boundary faces, and possibly one or more interfaces in the case of a multi-material corner.

Extended boundary and interface condition matrix. In these cases, the boundary and interface condition matrices, defined in Sections 3.3 and 3.5, are assembled in a $12W \times 12W$ real-valued *extended matrix of boundary and interface conditions for an open multi-material corner*

$$\mathbf{D}_{\text{corner_ext.}}(\vartheta, \omega, \mu) = \text{blocked_diag}[\mathbf{D}_{\text{BC}}(\vartheta_0), \mathbf{D}_{\text{I}}(\vartheta_1), \dots, \mathbf{D}_{\text{BC}}(\vartheta_W)] = \begin{bmatrix} \mathbf{D}_{\text{BC}}(\vartheta_0) & \mathbf{0}_{6 \times 12} & \mathbf{0}_{6 \times 12} & \cdots & \mathbf{0}_{6 \times 6} \\ \mathbf{0}_{12 \times 6} & \mathbf{D}_{\text{I}}(\vartheta_1) & \mathbf{0}_{12 \times 12} & \cdots & \mathbf{0}_{12 \times 6} \\ \vdots & \vdots & \vdots & \ddots & \vdots \\ \mathbf{0}_{6 \times 6} & \mathbf{0}_{6 \times 12} & \mathbf{0}_{6 \times 12} & \cdots & \mathbf{D}_{\text{BC}}(\vartheta_W) \end{bmatrix}. \quad (57)$$

It is evident that this matrix is an orthogonal matrix satisfying (53), in view of the orthogonality of the sub-matrices \mathbf{D}_{BC} and \mathbf{D}_{I} on its diagonal. For the sake of notation simplicity, on the right side of (57) the arguments ω, μ are omitted.

Open-corner characteristic matrix. As in (32) and (46), multiplying the vector $\mathbf{w}_{\text{corner_ext}}$ (51) by the matrix (57),

$$\mathbf{D}_{\text{corner_ext.}}(\vartheta, \omega, \mu) \mathbf{w}_{\text{corner_ext.}} = \mathbf{w}_{\text{corner_PU}} \quad (58)$$

we get a vector which can be split in the sub-vectors of the prescribed and unknown elastic variables at angles of wedge faces,

$$\mathbf{w}_{\text{corner_PU}} = \begin{bmatrix} \mathbf{w}_P(r, \vartheta_0) \\ \mathbf{w}_U(r, \vartheta_0) \\ \mathbf{w}_P(r, \vartheta_1) \\ \mathbf{w}_U(r, \vartheta_1) \\ \vdots \\ \mathbf{w}_P(r, \vartheta_W) \\ \mathbf{w}_U(r, \vartheta_W) \end{bmatrix}, \quad (59)$$

The size of the vector

$$\mathbf{w}_{\text{corner_U}} = \begin{bmatrix} \mathbf{w}_U(r, \vartheta_0) \\ \mathbf{w}_U(r, \vartheta_1) \\ \vdots \\ \mathbf{w}_U(r, \vartheta_W) \end{bmatrix} \quad (60)$$

obtained by omitting the prescribed zero values of the elastic variables, is $(6W - F) \times 1$, showing its dependence on the number of frictional sliding boundary and interface conditions, F . The relation (58), can be rewritten as

$$\mathbf{w}_{\text{corner_ext.}} = \mathbf{D}_{\text{corner_ext.}}^T(\vartheta, \omega, \mu) \mathbf{w}_{\text{corner_PU}} \quad (61)$$

by applying the orthogonality relation in (53). Substituting (61) into (52), we get

$$\mathbf{K}_{\text{corner_ext.}}(\lambda)\mathbf{D}_{\text{corner_ext.}}^T(\vartheta, \omega, \mu)\mathbf{w}_{\text{corner_PU}} = \mathbf{0}_{6W \times 1}. \quad (62)$$

Some columns of the matrix result of multiplying the first two terms of the previous expression can be removed as they would be multiplied by the prescribed zero values of $\mathbf{w}_p(r, \vartheta_w)$. This reduced, in general complex-valued, matrix has the following form

$$\mathbf{K}_{\text{corner}}(\lambda, \omega) = \begin{bmatrix} \mathbf{K}_1 \tilde{\mathbf{D}}_{\text{BC}}^T(\vartheta_0) & -\tilde{\mathbf{D}}_1^T(\vartheta_1) & \mathbf{0}_{6 \times n_2} & \cdots & \mathbf{0}_{6 \times n_{W-1}} & \mathbf{0}_{6 \times n_W} \\ \mathbf{0}_{6 \times n_0} & \mathbf{K}_2 \tilde{\mathbf{D}}_2^T(\vartheta_1) & -\tilde{\mathbf{D}}_1^T(\vartheta_2) & \cdots & \mathbf{0}_{6 \times n_{W-1}} & \mathbf{0}_{6 \times n_W} \\ \vdots & \vdots & \vdots & \ddots & \vdots & \vdots \\ \mathbf{0}_{6 \times n_0} & \mathbf{0}_{6 \times n_1} & \mathbf{0}_{6 \times n_2} & \cdots & \mathbf{K}_W \tilde{\mathbf{D}}_2^T(\vartheta_{W-1}) & -\tilde{\mathbf{D}}_{\text{BC}}^T(\vartheta_W) \end{bmatrix}, \quad (63)$$

where n_w is the number of rows in the matrices $\tilde{\mathbf{D}}_{\text{BC}}(\vartheta_w)$, for the boundary conditions on faces $w = 0$ and $w = W$, and the number of rows in the matrices $\tilde{\mathbf{D}}_i(\vartheta_w)$, for the interface condition matrices in $1 \leq w \leq W - 1$ and $i = 1, 2$. The number of rows in each case will depend on whether or not the frictional sliding contact condition is prescribed on a boundary face (i.e., $n_w = 2$ for frictional contact and $n_w = 3$ for other boundary conditions) or an interface (i.e., $n_w = 5$ for frictional contact and $n_w = 6$ for other interface conditions). In cases where $F = 0$, $\mathbf{K}_{\text{corner}}$ is a $6W \times 6W$ square matrix as in [18]. However, when a frictional sliding contact boundary or interface condition is prescribed on one or more material faces of the corner, $F \geq 1$, $\mathbf{K}_{\text{corner}}$ is a $6W \times (6W - F)$ rectangular matrix.

The application of (63) in (62) together with (60) leads to the *characteristic system for the singularity analysis of an open multi-material corner*, which represents a non-linear eigenvalue problem for this corner, for values λ and ω

$$\mathbf{K}_{\text{corner}}(\lambda, \omega)\mathbf{w}_{\text{corner_U}} = \mathbf{0}_{6W \times 1}. \quad (64)$$

The vector $\mathbf{w}_{\text{corner_U}}$ is an eigenvector that can be multiplied by any non-zero factor, remaining a solution of the eigenproblem. A value of this factor that makes that $\mathbf{w}_{\text{corner_U}}$ satisfies the compression condition on the surfaces with frictionless or frictional contact is chosen if possible.

4.2.2. Closed corner (periodic corner)

A closed corner, also called periodic corner, is a corner with no outer faces and including only interface conditions prescribed at angles $\vartheta_w (w = 0, \dots, W)$ where $\vartheta_W - \vartheta_0 = 360^\circ$.

Extended interface condition matrix. In this case, the interface condition matrices, defined in Section 3.5, are gathered in a $12W \times 12W$ real matrix,

$$\mathbf{D}_{\text{corner_ext.}}(\vartheta, \omega, \mu) = \begin{bmatrix} \mathbf{D}_2(\vartheta_0) & \mathbf{0}_{n'_0 \times 12} & \mathbf{0}_{n'_0 \times 12} & \cdots & \mathbf{0}_{n'_0 \times 12} & \mathbf{D}_1(\vartheta_W) \\ \tilde{\mathbf{D}}_2(\vartheta_0) & \mathbf{0}_{n_0 \times 12} & \mathbf{0}_{n_0 \times 12} & \cdots & \mathbf{0}_{n_0 \times 12} & \tilde{\mathbf{D}}_1(\vartheta_W) \\ \mathbf{0}_{12 \times 6} & \mathbf{D}_1(\vartheta_1) & \mathbf{0}_{12 \times 12} & \cdots & \mathbf{0}_{12 \times 12} & \mathbf{0}_{12 \times 6} \\ \vdots & \vdots & \vdots & \ddots & \vdots & \vdots \\ \mathbf{0}_{12 \times 6} & \mathbf{0}_{12 \times 12} & \mathbf{0}_{12 \times 12} & \cdots & \mathbf{D}_1(\vartheta_{W-1}) & \mathbf{0}_{12 \times 6} \end{bmatrix}, \quad (65)$$

called *extended matrix of interface conditions for a closed multi-material corner*. Recall that the interface condition at ϑ_0 is the same as the interface condition at ϑ_W , since $\vartheta_W - \vartheta_0 = 360^\circ$. In this matrix, $n_0 = n_W$ is the number of rows of $\tilde{\mathbf{D}}_i(\vartheta_w)$ and $n'_0 = n'_W$ is the number of rows of $\mathbf{D}_i(\vartheta_w)$, for $w = 0$ and W . Thus, $n_0 + n'_0 = 12$, keeping $\mathbf{D}_{\text{corner_ext.}}$ as a $12W \times 12W$ square matrix. For frictional contact at $w = 0$ and W , $n_0 = 5$, but for other interface conditions $n_0 = 6$. From the orthogonality relationship in (45), it can be deduced that this matrix is an orthogonal matrix, in a similar way as it was proved in [18, Appendix C].

Closed-corner characteristic matrix. Similar to open corners, if the vector $\mathbf{w}_{\text{corner_ext.}}$ is multiplied from the left by the matrix $\mathbf{D}_{\text{corner_ext.}}$, it is reordered in the vector $\mathbf{w}_{\text{corner_PU}}$ of prescribed and unknown variables

$$\mathbf{w}_{\text{corner_PU}} = \mathbf{D}_{\text{corner_ext.}}(\vartheta, \omega, \mu)\mathbf{w}_{\text{corner_ext.}}, \quad (66)$$

where \mathbf{w}_{PU} is the $12W \times 1$ vector

$$\mathbf{w}_{\text{corner_PU}} = \begin{bmatrix} \mathbf{w}_p(r, \vartheta_0) \\ \mathbf{w}_U(r, \vartheta_0) \\ \mathbf{w}_p(r, \vartheta_1) \\ \mathbf{w}_U(r, \vartheta_1) \\ \vdots \\ \mathbf{w}_p(r, \vartheta_{W-1}) \\ \mathbf{w}_U(r, \vartheta_{W-1}) \end{bmatrix}, \quad (67)$$

that can be reduced to a $(6W - F) \times 1$ vector

$$\mathbf{w}_{\text{corner_U}} = \begin{bmatrix} \mathbf{w}_U(r, \vartheta_0) \\ \mathbf{w}_U(r, \vartheta_1) \\ \vdots \\ \mathbf{w}_U(r, \vartheta_{W-1}) \end{bmatrix}, \quad (68)$$

of the unknown elastic variables, by omitting the prescribed zero values of the elastic variables.

Taking advantage of the orthogonality property of the matrix $\mathbf{D}_{\text{corner_ext.}}(\vartheta, \omega)$, the expression (66) can be rewritten as

$$\mathbf{w}_{\text{corner_ext.}} = \mathbf{D}_{\text{corner_ext.}}^T(\vartheta, \omega, \mu)\mathbf{w}_{\text{corner_PU}}. \quad (69)$$

Substituting this relation into (52) the following expression is obtained

$$\mathbf{K}_{\text{corner_ext.}}(\lambda)\mathbf{D}_{\text{corner_ext.}}^T(\vartheta, \omega, \mu)\mathbf{w}_{\text{corner_PU}} = \mathbf{0}_{6W \times 1}. \quad (70)$$

Knowing that some values of the vector $\mathbf{w}_{\text{corner_PU}}$ are the prescribed zero values, \mathbf{w}_p , some columns of the matrix which is the result of multiplying $\mathbf{K}_{\text{corner_ext.}}(\lambda)$ by $\mathbf{D}_{\text{corner_ext.}}^T(\vartheta, \omega, \mu)$ can be removed. This leads to a reduced $6W \times (6W - F)$, in general, complex-valued matrix

$$\mathbf{K}_{\text{corner}}(\lambda, \omega) = \begin{bmatrix} \mathbf{K}_1 \tilde{\mathbf{D}}_2^T(\vartheta_0) & -\tilde{\mathbf{D}}_1^T(\vartheta_1) & \mathbf{0}_{6 \times n_2} & \cdots & \mathbf{0}_{6 \times n_{W-2}} & \mathbf{0}_{6 \times n_{W-1}} \\ \mathbf{0}_{6 \times n_0} & \mathbf{K}_2 \tilde{\mathbf{D}}_2^T(\vartheta_1) & -\tilde{\mathbf{D}}_1^T(\vartheta_2) & \cdots & \mathbf{0}_{6 \times n_{W-2}} & \mathbf{0}_{6 \times n_{W-1}} \\ \vdots & \vdots & \vdots & \ddots & \vdots & \vdots \\ \mathbf{0}_{6 \times n_0} & \mathbf{0}_{6 \times n_1} & \mathbf{0}_{6 \times n_2} & \cdots & \mathbf{K}_{W-1} \tilde{\mathbf{D}}_2^T(\vartheta_{W-2}) & -\tilde{\mathbf{D}}_1^T(\vartheta_{W-1}) \\ -\tilde{\mathbf{D}}_1^T(\vartheta_0) & \mathbf{0}_{6 \times n_1} & \mathbf{0}_{6 \times n_2} & \cdots & \mathbf{0}_{6 \times n_{W-2}} & \mathbf{K}_W \tilde{\mathbf{D}}_2^T(\vartheta_{W-1}) \end{bmatrix}, \quad (71)$$

where n_w is the number of rows in the matrices $\tilde{\mathbf{D}}_i(\vartheta_w)$, for $0 \leq w \leq W - 1$ and $i = 1, 2$. Thus, $n_w = 5$ for friction interfaces and $n_w = 6$ for other interface conditions.

This reduced matrix appears in the *characteristic system for the singularity analysis of a closed multi-material corner*, which represents a non-linear eigenvalue problem for this corner, for unknown values λ and ω :

$$\mathbf{K}_{\text{corner}}(\lambda, \omega)\mathbf{w}_{\text{corner_U}} = \mathbf{0}_{6W \times 1}. \quad (72)$$

In cases where $F = 0$, $\mathbf{K}_{\text{corner}}$ is a $6W \times 6W$ square matrix, recovering the system deduced in [18]. However, when a frictional contact boundary or interface condition is prescribed on one or more corner faces, $F \geq 1$, $\mathbf{K}_{\text{corner}}$ is a $6W \times (6W - F)$ rectangular matrix.

As it may not be an easy task to deduce the matrix defined in (71) for the case of single wedge corners, the procedure to get the expressions for $\mathbf{K}_{\text{corner}}(\lambda, \omega)$ in the two possible cases was explained in [18, Eq. (88)] for a perfectly bonded corner and [18, Eq. (93)] for a closed corner with one frictionless sliding contact interface. The latter expression is also valid for the frictional sliding contact case, so it is not repeated here.

As in the open corner case, an eigensolution $\mathbf{w}_{\text{corner}_U}$ multiplied by any non-zero factor solves the system (72). As we need to check that compression is present on all contact faces, if in the obtained solution tension is obtained on all these contact faces, the solution can be multiplied by -1 to have compression on all these faces. If compression and tension are present on two different contact faces, such eigensolution is not valid.

4.3. Solution of the characteristic system. Singular elastic solution

The sought solution of the non-linear eigensystems in (64) or (72) is a (right) null vector of the matrix $\mathbf{K}_{\text{corner}}(\lambda, \omega)$, ignoring the trivial solutions with $\mathbf{w}_{\text{corner}_U} = \mathbf{0}$. This means that the next step is to find the *characteristic (singular) values of λ and ω* .

In the simplest case, for corners where $F = 0$, the matrix $\mathbf{K}_{\text{corner}}$ is a square matrix and λ is the only unknown. To obtain the λ values, solutions of the *characteristic equation of the corner*, the roots of the determinant of the matrix $\mathbf{K}_{\text{corner}}$ can be found

$$\det \mathbf{K}_{\text{corner}}(\lambda) = 0. \quad (73)$$

In general the roots of (73) can be real or complex. If λ is a complex root of (73) its complex conjugate is also a root of (73).

For corners where $F \geq 1$, a pair of values of λ and ω , non-trivial solution of the over-determined homogeneous systems (64) or (72), for open or closed corners, respectively, should be found. In the following, three different ways to get the values of λ and ω are proposed. In the first method the characteristic equation of the corner is written as a condition for a vanishing determinant

$$\det(\bar{\mathbf{K}}_{\text{corner}}^T(\lambda, \omega)\mathbf{K}_{\text{corner}}(\lambda, \omega)) = 0, \quad (74)$$

which ensures that the columns of $\mathbf{K}_{\text{corner}}$ are linearly dependent. This procedure has the advantage that the solution can be found in a similar way as in (73), but a disadvantage is that the algebraic multiplicity of each root is doubled. The second method is to evaluate the singular value decomposition (SVD) [44] of the matrix $\mathbf{K}_{\text{corner}}(\lambda, \omega)$ in (64) or (72), and to search for the vanishing minimum singular value by solving

$$\sigma_{\min}(\mathbf{K}_{\text{corner}}(\lambda, \omega)) = 0. \quad (75)$$

The last proposed method is to solve the following non-linear system of $6W$ equations

$$f(\mathbf{X}) = \mathbf{K}_{\text{corner}}(\lambda, \omega)\mathbf{w}_{\text{corner}_U} = \mathbf{0} \quad (76)$$

for $(6W + 1) \times 1$ vector of unknowns

$$\mathbf{X} = \begin{bmatrix} \mathbf{w}_{\text{corner}_U} \\ \lambda \\ \omega \end{bmatrix}. \quad (77)$$

This non-linear system could be augmented by a normalisation condition for $\mathbf{w}_{\text{corner}_U}$ leading to a system with the same number of equations and unknowns.

Usually, the characteristic values of λ are searched in the range $0 \leq \text{Re}(\lambda) \leq 1$, as those singularity exponents λ correspond to singular elastic solutions in the corner with unbounded stresses and strains at the corner tip, but with a finite elastic strain energy there. The characteristic values of ω are searched in the range $-180^\circ \leq \omega_{k_i} \leq 180^\circ$, for each component ($i = 1, \dots, F$). Recall that one ω_{k_i} value is found per each interface or boundary face where a frictional contact is considered.

Once the values of λ and ω , the solution to the corner problem, are obtained, the singular stress and displacement fields can be computed using the same procedure as in [18, Section 6].

Once displacements and stresses are obtained for a pair (λ, ω) , it is possible to check the feasibility of the eigensolution by verifying the compression condition on the contact surfaces and the condition of frictional energy dissipation. If the computed relative sliding direction

and the shear stress vector direction are parallel but with opposite directions, the frictional energy dissipation condition is fulfilled. This does not necessarily mean that eigensolutions which do not verify this condition cannot be useful, given that the friction energy dissipation condition is strictly speaking written in terms of the variation of relative displacement, not its value. Therefore, in some configurations such eigensolutions could be superposed with other solutions leading to fulfilment of the friction energy dissipation condition.

Significant observations on the possibility of obtaining a complex singularity exponent $\lambda \in \mathbb{C}$, and its implications in configurations involving frictional contact are presented in Section 7.

5. MATLAB implementation

New functions needed to cover the case of corners with frictional sliding contact on outer boundaries and interface are added to the code developed in [18] for corners with homogeneous boundary and interface conditions. The resulting code is organised in 6 modules similar to [18, Section 7.1], thus only the relevant changes in the code are mentioned in the following

- **Data input** Friction coefficient can be introduced for some corner surfaces.
- **Definition of single-material wedges**
- **Boundary and interface condition matrices** The matrices described in Tables 1 and 2 are added for some corner surfaces.
- **Characteristic system assembly** The main difference is the possibility that the matrix $\mathbf{K}_{\text{corner}}$ is a rectangular matrix, which depends not only on λ , but also on as many angles ω_{k_i} as faces with frictional sliding contact exist in the corner.
- **Solution of the characteristic system** This module involves the most substantial changes. A new sub-module is developed for corners with frictional contacts. The non-linear eigensystem to be solved depends on the characteristic pair (λ, ω) . In the most common and simplest case, when there is only one frictional contact, to help find the initial point for the search for the solution of (74), (75) or (76) a contour plot of values of $\sigma_{\min}(\lambda, \omega)$ for $0 \leq \lambda \leq 1$ and $-\pi \leq \omega \leq \pi$ is computed, as shown in Fig. 6. In this plot the user can search manually for pairs of values of λ and ω that make the value of $\sigma_{\min}(\lambda, \omega)$ close to zero. These values are used as a starting point to find the solution of (76) with the Levenberg–Marquardt algorithm. With this algorithm, it is possible to find real and complex values of λ . The reason to use the third method (76) from those presented in Section 4.3, is that after several tests done with Matlab, this method tends to converge to a more accurate solution than the methods based on (74) and (75).

In some cases where frictional contact is imposed, the presented algorithm converges to $\lambda \in \mathbb{C}$. In these cases, when $\omega \in \mathbb{R}$, typically $\omega = 0, 180^\circ$, the results obtained with the code are valid, but when $\omega \neq 0, 180^\circ$, the code cannot separate the real part of the solution from the imaginary part and $\omega \in \mathbb{C}$ is obtained. This solution is not valid, and the corner singularity problem needs to be solved by a different procedure currently under development and which will be presented in a forthcoming work.

- **Displacement and stress singular fields** This module requires to additionally substitute the value of ω in (64) or (72) and take into account the modified size of the boundary and interface matrices in the case of frictional contact.

Table 3
Engineering constants for the linear elastic materials used in the studied examples. Elastic moduli and shear moduli in GPa and fibre angles ϕ_i in degree.

Material	E_1	E_2	E_3	G_{12}	G_{13}	G_{23}	ν_{12}	ν_{13}	ν_{23}	ϕ_i
A	68.67						0.33			
B	3						0.35			
C	137.89	14.48	1	5.86	1	1	0.21	0	0	0
D	137.9	14.48	14.48	5.86	5.86	5.86	0.21	0.21	0.21	ϕ_i
E	137.9	14.48	14.48	4.98	4.98	4.98	0.21	0.21	0.21	ϕ_i
F	5.85						0.25			
G	141.3	9.58	9.58	5	5	3.5	0.3	0.3	0.32	ϕ_i

6. Numerical examples

Following the tests carried out in [18], the matrix formalism and the code developed in the present article are checked by comparing its results with those available in the literature. In Table 3, the engineering constants for the materials used in the examples are listed in the full precision used.

In the numerical examples, the boundary condition (BC) used are stress-free (F), clamped (C), symmetry (frictionless contact) (S), antisymmetry (A) and frictional contact (FC). The interface condition (IC) are perfectly bonded (B), frictionless interface (FL) and frictional contact (FC).

The abbreviation ‘‘Ex’’ stands for the number of each example and is indicated in the corresponding column of each table when it contains more than one example or in the title of the table or figure when it contains only one example. For cases with boundary faces or interfaces with frictional contact, $f \leq 0$ is used if the authors do so in their articles and in that case $\mu = |f|$. The symbol ϕ_i corresponds to the rotation angle around the x_i -axis of the composite material fibre, see Fig. 5. If the composite material has the fibres lying on the x_1x_3 -plane and parallel to x_1 or x_3 -axis the material behaves as an orthotropic material, if the fibre is lying on the x_1x_3 or x_1x_2 -plane rotated around the x_2 or x_3 -axis respectively an angle ϕ_i , black lines in Fig. 5, the composite material behaves as an apparently monoclinic material, and if the composite material has the fibre as the red line in Fig. 5, it behaves as an apparently anisotropic material. As remarked in the previous sections, once the λ and ω solutions in the studied problems are computed, it is necessary to check if the relative tangential displacement obtained and the friction shear stress satisfy the friction dissipation condition, having both the same direction but opposite orientation, expressions (21) and (38). Eigensolutions that meet the frictional dissipation of energy requirement are marked with (*), and with (o) for solutions with no frictional tangential stress at the interface, including anti-plane mode. It must also be checked if the compression condition $\sigma_{\theta\theta} \leq 0$ is satisfied on the contact face. When this condition is not satisfied, the solution is marked with the symbol (\pm), which means that one contact face is under compression and the other face is under tension. In the examples shown in this section, the number of faces with frictional contact is $F=1$, except in examples 1.9, 1.14 and 4 where $F = 2$. Noteworthy, problems with $F > 2$ can be solved with the present matrix formalism and the developed computational code, but the authors have not found any previously solved problems with more than two friction contact surfaces in the literature, so a comparison is not possible.

6.1. Singular solutions for open corners

6.1.1. Singular solutions for open corners with only one single-material wedge

Example 1.1 - 1.4. For corners made of a single material, $\mathbf{K}_1 = \mathbf{E}_1$, Table 4 presents the results for an isotropic wedge with different values of angles θ_1 and different boundary conditions, one of them being frictional sliding contact. These results are compared with those obtained using the closed-form eigenequations by Sinclair [5], who observed that both positive and negative friction coefficients $f \leq 0$ should be tried to ensure that the shear stress opposes any sliding, i.e., ensure the frictional dissipation of energy condition. This can

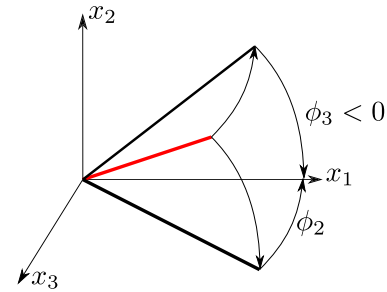


Fig. 5. Fibre position for apparently anisotropic material.

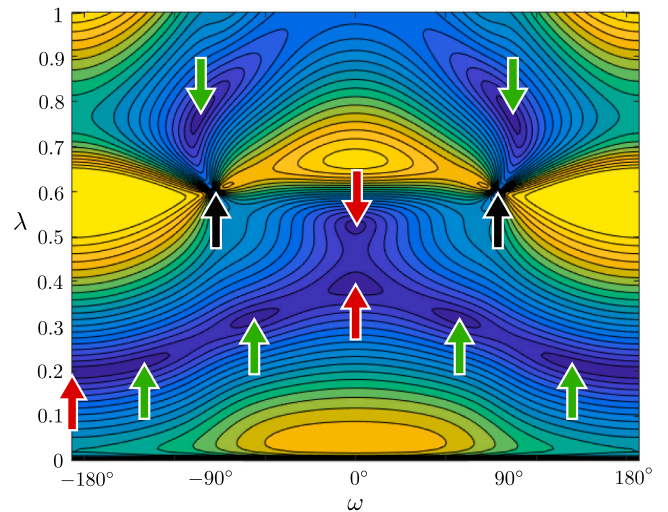
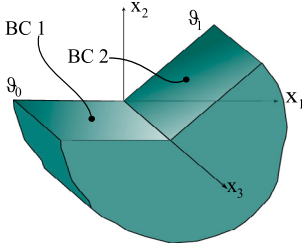


Fig. 6. Contour plot of σ_{\min} values of the SVD of the matrix $\mathbf{K}_{\text{corner}}$ in Examples 1.1, for $0 \leq \lambda \leq 1$ and $-\pi \leq \omega \leq \pi$. Red arrows are solutions found also solving eigenequation from [5], black arrows are solutions that match with the anti-plane mode and green arrows are unexpected solutions.

be achieved by selecting the appropriate sign of f . With the present formalism, with $\mu \geq 0$, we can find the results for both signs of f computed with the closed-form expressions found in [5] considering $-\pi \leq \omega \leq \pi$. Solutions in [5] correspond to the plane mode and coincide up to more than 9 decimal places with the results obtained with the present code. Furthermore, this present methodology allows us to find the solutions corresponding to the anti-plane mode, those with $\omega = \pm 90^\circ$, as well as some unexpected solutions, those with $\omega \neq 0^\circ, \pm 90^\circ, 180^\circ$, that involve modes in which the plane and anti-plane modes cannot be decoupled. To the best of the authors’ knowledge, these cases have not been previously reported by any other author for either isotropic or orthotropic materials, and their existence and properties will be studied in depth in a forthcoming article. The case with both boundaries of the corner having frictional sliding boundary condition with $\mu = 1$ is computed for a wedge angle of 300° . The results obtained are the same as those for a wedge angle of 150° with a frictional sliding boundary condition on one face and symmetry or

Table 4

Comparison of results for $0 \leq \lambda \leq 1$ and ω obtained by the present code and those found in the literature, for open single-material isotropic corners with one frictional boundary condition, Section 6.1.1. (*) Fulfills the frictional dissipation of energy condition. (o) No frictional tangential stress on the contact face, including anti-plane mode.

Corner configuration	Ex.	BC1	BC2	Mat	Results in literature [5]	Present results λ, ω	
	1.1	FC $\mu = 1$ $\vartheta_0 = 0^\circ$	F $\vartheta_1 = 300^\circ$	A	0.3916876291	0.3916876291	
					$f = 1$	0.0°	
					0.5238206585	0.5238206585	
					$f = 1$	0.0°	
					-	0.3168546234 65.645°	
					-	0.3168546234 -65.645°	
					-	0.6, 90.0° (o)	
					-	0.6, -90.0° (o)	
					-	0.7694649581 98.480° (*)	
					-	0.7694649581 -98.480° (*)	
					-	0.209797619 145.101°	
					-	0.209797619 -145.101°	
					-	0.1968137883 $f = -1$	0.1968137883 180.000° (*)
					1.2	FC $\mu = 1$ $\vartheta_0 = 0^\circ$	C $\vartheta_1 = 300^\circ$
$f = 1$	0.0° (*)						
0.649215698	0.649215698						
$f = 1$	0.0° (*)						
0.867301578	0.867301578						
$f = 1$	0.0°						
-	0.3, 90.0° (o)						
-	0.3, -90.0° (o)						
-	0.9, 90.0° (o)						
-	0.9, -90.0° (o)						
-	1 107.303° (*)						
-	1, -107.303° (*)						
-	0.297128929 $f = -1$	0.297128929 180.0°					
-	0.512105442 $f = -1$	0.512105442 180.0° (*)					
1.3	FC $\mu = 1$ $\vartheta_0 = 0^\circ$	S $\vartheta_1 = 150^\circ$	A	0.484725982	0.484725982		
				$f = 1$	0° (*)		
				0.760133083	0.760133083		
				$f = 1$	0°		
-	0.954171230 79.766°						
-	0.954171230 -79.766°						
1.4	FC $\mu = 1$ $\vartheta_0 = 0^\circ$	A $\vartheta_1 = 150^\circ$	A	0.245553923	0.245553923		
				$f = 1$	0°		
				-	0.285960827, 44.056°		
				-	0.285960827, -44.056°		
				-	0.6, 90.0° (o)		
-	0.6, -90.0° (o)						
-	0.533683783 $\pm 0.20979646i$ $f = -1$	0.533683783 $\pm 0.20979646i$ 180.0°					

antisymmetry boundary condition on the other face, Examples 1.3 and 1.4, respectively, in Table 4. The solution of Example 1.4 with $f = -1$ obtained by searching for roots of the closed-form corner-eigenequation given in [5] and also by the present formalism, with the angle $\omega = 180^\circ$,

gives a complex singularity exponent $\lambda \in \mathbb{C}$. This solution leads to an oscillatory stress field similar to the well-known oscillatory solution in the open model of an interface crack between dissimilar materials with the Dundurs parameter $\beta \neq 0$ as analysed in [45,46].

In Fig. 6, the contour plot of σ_{\min} values of the singular value decomposition (SVD) of the matrix $\mathbf{K}_{\text{corner}}(\lambda, \omega)$, matrix of the characteristic system for the singularity analysis, for the case in Example 1.1 is shown to illustrate how the solutions for λ and ω are found. The darker blue zones correspond to values of σ_{\min} close to 0, so the singularity exponent λ and the associated angle ω can be found there. The red arrows correspond to solutions found also solving eigenequation from [5], the black arrows are the solutions corresponding to the anti-plane mode and the green arrows are the unexpected solutions mentioned above. These latter values and their existence will be studied in a forthcoming article.

Example 1.5 - 1.14. For a single-material orthotropic corner, the results are compared with the results obtained by the closed-form expression of corner eigenequations deduced in [43]. These examples are shown in Table 5 for half-planes and in Table 6 for cracks with frictional-sliding-contact boundary conditions. The values of ϑ_0 and ϑ_1 used for the computation of the solution are indicated, but the results were checked to be valid for any combination of $\vartheta_1 - \vartheta_0 = 180^\circ$ in Table 5 and $\vartheta_1 - \vartheta_0 = 360^\circ$ in Table 6. Examples 1.9 and 1.14 represent the cases with frictional sliding contact on the two boundary faces. In these cases, the sliding (or shear) direction angles are shown for both faces, ω_0 and ω_1 . In [43] the closed-form expressions were deduced only for the plane mode, in Tables 5 and 6 the results obtained by the present code corresponding to the anti-plane mode ($\omega = \pm 90^\circ$) and modes in which the plane and anti-plane modes cannot be decoupled ($\omega \neq 0^\circ, \pm 90^\circ, 180^\circ$) are also presented. Any combination of $\lambda, \omega_0, \omega_1$ values that satisfies the conditions $\lambda \in \mathbb{Z}$, i.e. λ is an integer number, and $\omega_1 = -\omega_0 \pm n\pi$, with $n \in \mathbb{Z}$, is also a solution of Example 1.9. Example 1.8 corresponds to an orthotropic semi-plane with antisymmetric boundary condition at ϑ_0 and frictional sliding contact at ϑ_1 , the same boundary condition as in Examples 1.4, resulting in a solution with complex singularity exponent $\lambda \in \mathbb{C}$ also. In all examples, the compression condition at the frictional contact boundary is checked. As Examples 1.9 and 1.14 have frictional contact on both boundaries, both outer faces must simultaneously fulfil the compression condition. However, this requirement is not satisfied by the solutions marked with (\pm) in Tables 5 and 6. In Table 6 some λ values are solution of the problem regardless of the value of ω , this is indicated as $\forall \omega$ in the table.

6.1.2. Singular solution for open corners with two single-material wedges

Example 2.1. Gdoutos and Theocaris [47], employing the Williams [48] technique, deduced a corner eigenequation to study the existence of a power singularity at the apex of a plane indenter acting on an elastic half-plane, applying the Dundurs mismatch parameter β for bi-material isotropic corners for different values of the friction coefficient and the sharp edge angle. This eigenequation [47, Eq. (3)] is implemented to obtain the singularity exponent for the friction coefficients $f = -1, -0.5, 0, 0.5$, and 1 , and the solid angles of the indenter, $\vartheta = 30^\circ, 45^\circ, 60^\circ, 90^\circ$ and 120° . The material used for the half plane is B and for the indenter is A in Table 3. All results obtained by solving the corner eigenequation [47, Eq. (3)] are compared with the results obtained for each case by the present general matrix formalism with perfect match at least up to 12 digits. Later, Comninou [23] studied the same case, but employing the Mellin transform that essentially leads to the same expression of eigenequation as in [47] and therefore to the same results. In Table 7 some of the results obtained are shown. The results shown for a friction coefficient $\mu = 0$ have been obtained in two different ways with the present formalism for verification purposes. First, using the interface condition matrices considering specifically the frictionless case as presented in [18], and then with the interface condition matrices in Table 2 considering $\mu = 0$ obtaining identical results up to 12 digits.

Examples 2.2 and 2.3. Churchman and Hills [27] present a simpler corner eigenequation for the same case as in Example 2.1 but in isotropic corners with the same materials and $\vartheta_2 = 90^\circ$ angle of indenter. In this kind of problem, as both wedges are made of the same material, the results are independent of the properties of the material. In Fig. 7, the results λ and ω obtained with the present formalism are superimposed on the Fig. 3 in [27], and the numerical results are presented in Table 8. The positive values of $-f$ in Fig. 7 correspond to $\omega = 180^\circ$ in Table 8 and the negative values of $-f$ correspond to $\omega = 0^\circ$. As can be seen in both Fig. 7 and Table 8, for the case of a perfectly bonded interface, the singular exponents obtained are the same as those that can be obtained for a friction coefficient $\mu = 0.219$ and a sliding angle $\omega = 0^\circ$ and for $\mu = 0.543$ and a sliding angle $\omega = 180^\circ$. Thus, $\mu = 0.219$ and $\mu = 0.543$ are considered limit cases where there is no sliding. This case can be instructive to show why, when varying the friction coefficient, a solution becomes invalid as it is not fulfilling the frictional dissipation of energy condition.

Hong et al. [30] presented a particularisation of the eigenequation introduced by Gdoutos and Theocaris [47] and Comninou [23] for the case of a quarter-plane sliding with or without friction over a semi-plane. The results obtained with the characteristic eigenequation (8) in [30] is successfully verified with the present formalism. Characteristic eigenequation (9) in [30] has also been verified for the case of a perfectly bonded interface. Yang in [29] presented solutions to dissimilar material contact problems. In this case, both wedges in contact can vary their solid angle and the interface condition allows friction. Eigenequation (58) in [29] is implemented and validated by comparing its solutions with the result obtained for the same configurations with the present general matrix formalism. For the tests, materials A and B have been used with varying solid angles for both materials and the friction coefficient.

Example 2.4. For the case of anisotropic materials, several procedures can be found in the literature. Chen et al. [36] proposed a new specific semi-analytic approach based on the Stroh formalism for frictional sliding contact of two anisotropic wedges considering GPS and the isotropic Coulomb frictional contact law at the interface. Despite the use of a similar friction model, the present results shown in Table 9 do not match with their results. In Fig. 8, the values for $\delta = \lambda - 1$ in Table 9 are superimposed with the results obtained in [36, Fig. 5], using the same colours for each friction coefficient, to show the differences between the results found in [36] and those obtained with the present formalism. In Fig. 8 only results that satisfy the frictional dissipation of energy condition and results of the frictionless case are plotted to make the figure clearer. The most striking difference is that for all values of the friction coefficient, the results shown in [36, Fig. 5] tend to $\delta = -0.5$ ($\lambda = 0.5$), a characteristic that is not found in the values obtained by the present formalism. In each column in Table 9, results for each friction coefficient at the interface are presented for different wedge angles of the upper material. Material E in Table 3 is used for the half-plane and for the wedge. The fibre angles are $\phi_2^1 = 45^\circ$ and $\phi_2^2 = -45^\circ$ for the half-plane and wedge, respectively. In [49] a generalisation of the semi-analytic approach introduced in [36], considering general boundary conditions on the outer faces, is developed and implemented in a computational code, providing the same results as obtained with the present general matrix formalism. In view of all this, we are fully confident in our results shown in Fig. 8 and Table 9 as we obtain them in two different ways. It has been observed that singular solutions with $\lambda \in \mathbb{C}$ may exist for some combinations of the friction coefficient μ and the wedge angle θ , but as these solutions are out of the scope of this work, we have not included them either in Table 9 or in Fig. 8.

Example 2.5. Poonsawat et al. [31], use a frictional model in which the relative displacement between the crack faces in the x_3 -direction is not allowed, which apparently does not represent the standard Coulomb isotropic friction law, as in general the collinearity of the friction shear vector and the vector of relative tangential displacement is not verified.

Table 5

Comparison of results for $0 \leq \lambda \leq 1$ and ω obtained by the present code and those found in the literature, for open single-material orthotropic corners with at least one frictional boundary condition, Section 6.1.1. (*) Fulfills the frictional dissipation of energy condition. (o) No frictional tangential stress on the contact face, including anti-plane mode. (\pm) One contact face under compression and the other contact face under tension.

Corner configuration	Ex.	BC1	BC2	Mat	Results in literature [43] λ, f	Present results λ, ω
					0.423597837	0.423597837
					$f = 1$	0° (*)
					–	0.479710607
					–	$\pm 71.58632^\circ$ (*)
	1.5	F $\theta_0 = 20^\circ$	FC $\mu = 1$ $\theta_1 = 200^\circ$	C	–	0.520289393
					–	$\pm 111.78927^\circ$
					0.547802109	0.547802109
					$f = -1$	$\pm 180^\circ$
					0.423597837	0.423597837
					$f = 1$	0°
	1.6	C $\theta_0 = 20^\circ$	FC $\mu = 1$ $\theta_1 = 200^\circ$	C	–	$0.5 \pm 90^\circ$ (o)
					0.547802109	0.547802109
					$f = -1$	$\pm 180^\circ$ (*)
					0.923597837	0.923597837
					$f = 1$	0°
	1.7	S $\theta_0 = 20^\circ$	FC $\mu = 1$ $\theta_1 = 200^\circ$	C	0.047802109	0.047802109
					$f = -1$	180° (*)
					0.461798918 \pm 0.1098658i	0.461798918 \pm 0.1098658i
					$f = 1$	0°
					–	$0.5 \pm 90^\circ$ (o)
					–	0.618471327
					–	$\pm 91.0944^\circ$ (*)
	1.8	A $\theta_0 = 20^\circ$	FC $\mu = 1$ $\theta_1 = 200^\circ$	C	–	0.3815286737
					–	$\pm 92.0756^\circ$
					0.707032932	0.707032932
					$f = -1$	180° (*)
					0.340769177	0.340769177
					$f = -1$	180°
					1 $f_1=1, f_2 = 1$	1 $\omega_0 = 0^\circ, \omega_1 = 0^\circ$
					0.875795728	0.875795728
					$f_1=-1, f_2 = 1$	$\omega_0 = 180^\circ, \omega_1 = 0^\circ$
	1.9	FC $\mu = 1$ $\theta_0 = 20^\circ$	FC $\mu = 1$ $\theta_1 = 200^\circ$	C	0.124204272	0.124204272
					$f_1=1, f_2 = -1$	$\omega_0 = 0^\circ, \omega_1 = 180^\circ$ (\pm)
					1, $f_1 = -1, f_2 = -1$	1, $\omega_0 = 180^\circ, \omega_1 = 180^\circ$

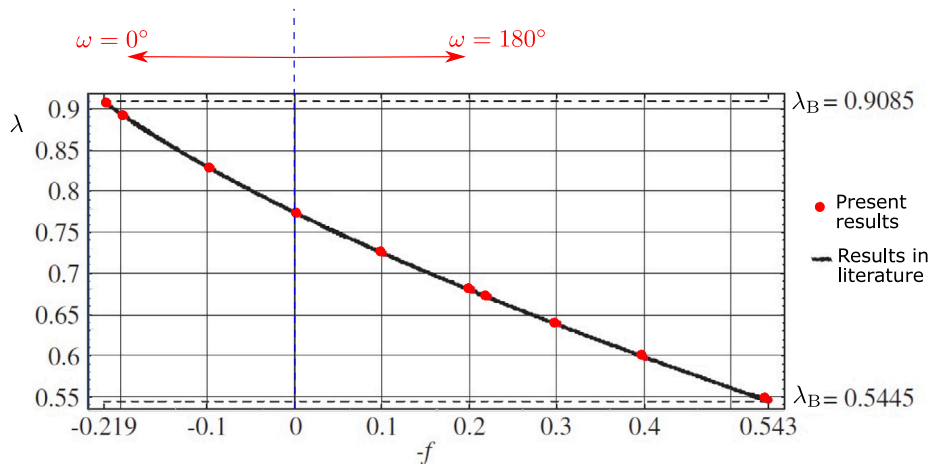
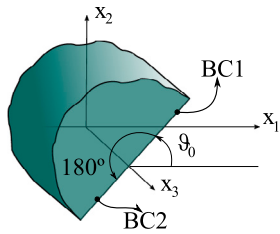


Fig. 7. $0 < \lambda < 1$ and ω results in Table 8 presented together with [27, Fig. 3]. λ_B with the eigenvalues plotted by Churchman and Hills [27] for the case of the bonded interface. See Ex 2.2 and Ex 2.3 in Table 8.

For that reason, the angle of the tangential frictional stress vector ω is not taken into account in [31], and our results only agree in those cases in which ω is either 0° or 180° . In Table 10, the variations of λ and ω with $\phi_2^{\text{Mat}_1}$ and $\phi_2^{\text{Mat}_2}$, for a friction coefficient $\mu = 0.5$, are

studied using the present friction model applied to the same problem as considered in [31, Tables 4 and 5], a 90° broken graphite/epoxy laminate ($\theta_0 = -180^\circ, \theta_1 = 0^\circ$ and $\theta_2 = 90^\circ$) shown in Fig. 9. The material used in [31] is the material D in Table 3. The shaded cells

Table 6

Comparison of results for $0 \leq \lambda \leq 1$ and ω obtained by the present code and those found in the literature, for open single-material orthotropic corners with at least one frictional boundary condition, Section 6.1.1. (*) Fulfills the frictional dissipation of energy condition. (o) No frictional tangential stress on the contact face, including anti-plane mode. (\pm) One contact face under compression and the other contact face under tension.

Corner configuration	Ex.	BC1	BC2	Mat	Results in literature [43] λ, f	Present results λ, ω
					0.5, $f = \pm 1$	0.5, $\forall \omega$ (o)
					0.222856347	0.222856347
					$f = 1$	0° (*)
					0.722856347	0.722856347
					$f = 1$	0° (*)
					-	0.240280639
						$\pm 69.204^\circ$ (*)
					-	0.740280639
						$\pm 69.204^\circ$ (*)
					-	0.259719361
						$\pm 110.800^\circ$
					-	0.759719361
						$\pm 110.800^\circ$
					0.277143653	0.277143653
					$f = -1$	180°
					0.777143653	0.777143653
					$f = -1$	180°
					0.222856347	0.222856347
					$f = 1$	0°
					0.5, $f = \pm 1$	0.5, $\forall \omega$ (o)
					0.722856347	0.722856347
					$f = 1$	0°
					-	0.25, 90° (o)
					-	0.75, 90° (o)
					0.277143653	0.277143653
					$f = -1$	180° (*)
					0.777143653	0.777143653
					$f = -1$	180° (*)
					0.472856347	0.472856347
					$f = 1$	0°
					0.5, $f = \pm 1$	0.5 $\forall \omega$ (o)
					0.972856347	0.972856347
					$f = 1$	0°
					0.027143653	0.027143653
					$f = -1$	180° (*)
					0.527143653	0.527143653
					$f = -1$	180° (*)
					0.222856347	0.222856347
					$f = 1$	0°
					0.25, $f = \pm 1$	0.25, $\forall \omega$ (o)
					0.722856347	0.722856347
					$f = 1$	0°
					0.75, $f = \pm 1$	0.75, $\forall \omega$ (o)
					0.277143653	0.277143653
					$f = -1$	180° (*)
					0.777143653	0.777143653
					$f = -1$	180° (*)
					0.5, $f_1 = 1,$ $f_2 = 1$	0.5, $\omega_0 = 0^\circ,$ $\omega_1 = 0^\circ$ (\pm)
					0.5, $f_1 = -1,$ $f_2 = 1$	0.5, $\omega_0 = 180^\circ,$ $\omega_1 = 0^\circ$ (o)
					0.445712694	0.445712694
					$f_1 = -1, f_2 = 1$	$\omega_0 = 180^\circ,$ $\omega_1 = 0^\circ$ (\pm)
					0.945712694	0.945712694
					$f_1 = -1, f_2 = 1$	$\omega_0 = 180^\circ, \omega_1 = 0^\circ$
					0.5, $f_1 = 1,$ $f_2 = -1$	0.5, $\omega_0 = 0^\circ,$ $\omega_1 = 180^\circ$ (o)

(continued on next page)

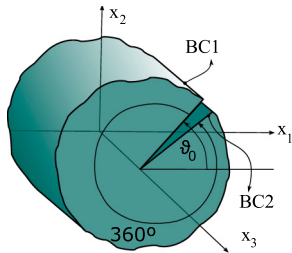


Table 6 (continued).

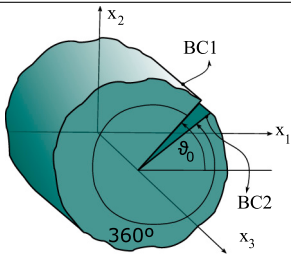
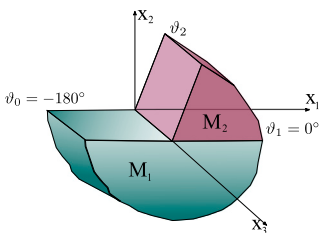
Corner configuration	Ex.	BC1	BC2	Mat	Results in literature [43] λ, f	Present results λ, ω
	1.14	FC $\mu = 1$ $\theta_0 = 0^\circ$	FC $\mu = 1$ $\theta_1 = 360^\circ$	C	0.054287306 $f_1 = 1, f_2 = -1$	$\omega_0 = 0^\circ,$ $\omega_1 = 180^\circ (*)$
					0.554287306 $f_1 = 1, f_2 = -1$	0.554287306 $\omega_0 = 0^\circ,$ $\omega_1 = 180^\circ (\pm)$
					0.5 $f_1 = -1,$ $f_2 = -1$	0.5, $\omega_0 = 180^\circ,$ $\omega_1 = 180^\circ (\pm)$

Table 7

Example 2.1. Comparison of results for $0 \leq \lambda \leq 1$ and ω obtained by the present code and those found in the literature for a wedge sliding with friction over a semi-plane. (*) Fulfills the frictional dissipation of energy condition.

Corner configuration	Mat	Ex.	BC1	IC1	BC2	Results in literature [23,47] λ, f	Present results λ, ω	
	2.1	$M_1 = A$ $M_2 = B$	F $\theta_0 = -180^\circ$		F $\theta_2 = 45^\circ$	0.829085095	0.829085095	
					FC $\mu = 0$ $\theta_1 = 0^\circ$	F $\theta_2 = 60^\circ$	0.629457434	0.629457434
						F $\theta_2 = 90^\circ$	0.526550237	0.526550237
						F $\theta_2 = 120^\circ$	0.505189351	0.505189351
						F $\theta_2 = 45^\circ$	0.978829646 $f = 0.5$	0.978829646 $0^\circ (*)$
					FC $\mu = 0.5$ $\theta_1 = 0^\circ$	F $\theta_2 = 60^\circ$	0.736972103 $f = -0.5$	0.736972103 $180^\circ (*)$
						F $\theta_2 = 90^\circ$	0.660673397 $f = 0.5$	0.660673397 0°
						F $\theta_2 = 60^\circ$	0.601424848 $f = -0.5$	0.601424848 $180^\circ (*)$
						F $\theta_2 = 90^\circ$	0.513745930 $f = 0.5$	0.513745930 0°
					FC $\mu = 1$ $\theta_1 = 0^\circ$	F $\theta_2 = 120^\circ$	0.538993666 $f = -0.5$	0.538993666 $180^\circ (*)$
						F $\theta_2 = 120^\circ$	0.478522170 $f = 0.5$	0.478522170 0°
						F $\theta_2 = 120^\circ$	0.531520587 $f = 0.5$	0.531520587 $180^\circ (*)$
						F $\theta_2 = 60^\circ$	0.697046375 $f = 1$	0.697046375 $0^\circ (*)$
					FC $\mu = 1$ $\theta_1 = 0^\circ$	F $\theta_2 = 60^\circ$	0.575440465 $f = -1$	0.575440465 $180^\circ (*)$
						F $\theta_2 = 90^\circ$	0.500701246 $f = 1$	0.500701246 0°
						F $\theta_2 = 90^\circ$	0.550975283 $f = -1$	0.550975283 $180^\circ (*)$
						F $\theta_2 = 120^\circ$	0.452032964 $f = 1$	0.452032964 0°

contain results obtained with the present code that match the results obtained by [31], taking into account that in [31, Tables 4 and 5] $k = 1 - \lambda$ is presented. Although, only two of the singular solutions with $0 < \lambda < 1$ presented in Table 10 fulfil the frictional dissipation of energy condition, it has been checked that solutions with $\lambda > 1$ can be found which fulfil this condition.

Magnier et al. [32] use the same frictional model as Poonsawat et al. [31] but a different computational procedure. To validate their methodology, Magnier et al. [32] reproduce the results presented in [31, Fig. 5, 6 and 7] for an inclined broken graphite/epoxy, material D in Table 3, indenting a semi-plane of the same material with good agreement. As their frictional model does not allow relative displacement in the x_3 -direction, only the results shown in [32] in Fig. 7 (a) with $[\phi^1/\phi^2] = [0^\circ/90^\circ]$ and (d) with $[\phi^1/\phi^2] = [90^\circ/0^\circ]$, and in Fig. 8 (a) with $[\phi^1/\phi^2] = [0^\circ/90^\circ]$ and (d) with $[\phi^1/\phi^2] = [90^\circ/0^\circ]$, agree with

the results obtained for the same problems using the present matrix formalism. That is, the same results are obtained only when the x_1x_2 -plane is a PES, and therefore $\omega = 0^\circ$ or 180° . Noteworthy, for the case of a perfectly bonded interface, all the results shown in [32, Fig. 6] coincide with the results by the present procedure.

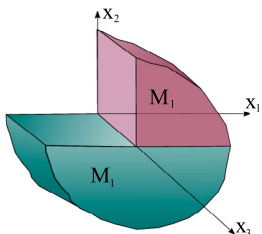
6.2. Singular solutions for closed (periodic) corners

6.2.1. Singular solutions for closed (periodic) corners with one multi-material wedge

Example 3.1. Frictional interface crack in an isotropic bi-material. Interface cracks with frictionless and frictional contact in isotropic bi-materials were first studied by Comninou [24,50]. The present results in Table 11 for the frictional interface crack are compared with the values of the singularity exponent λ given by the closed-form expression

Table 8

Numerical values for $0 < \lambda < 1$ and ω shown in Fig. 7, for open isotropic bi-material corners with frictional interface, see Section 6.1.2. (*) Fulfills the frictional dissipation of energy condition.

Corner configuration	Ex.	Mat	BC1	BC2	IC1 $\vartheta_1 = 0^\circ$	Present results λ, ω				
	2.2	A	F $\vartheta_0 = -180^\circ$	F $\vartheta_2 = 90^\circ$	FC $\mu = 0$	0.774013112 0° or 180°				
					FC $\mu = 0.1$	0.829259401 0° (*) 0.724882387 180°				
					FC $\mu = 0.2$	0.894461293 0° (*) 0.679923917 180°				
					FC $\mu = 0.219$	0.908587745 0° 0.671750475 180°				
					FC $\mu = 0.3$	0.979878330 0° 0.637987188 180°				
					FC $\mu = 0.4$	0.598318974 180°				
					FC $\mu = 0.543$	0.544511442 180°				
					2.3	A	F $\vartheta_0 = -180^\circ$	F $\vartheta_2 = 90^\circ$	B	0.544511442 0.908587745

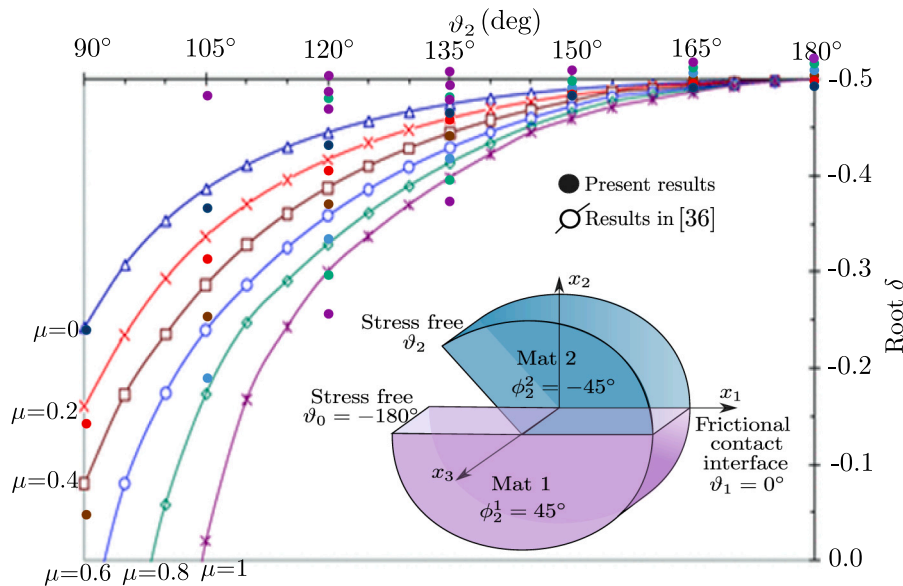


Fig. 8. Example 2.4. $\delta = \lambda - 1$ values versus upper wedge angle ϑ_2 for the case of a bi-material open corner with frictional contact interface presented in Table 9, superimposed with those obtained by Chen et al. [36, Fig. 5]. Mat. 1 and Mat. 2 are material E in Table 3, see Section 6.1.2.

deduced in [24]. The configuration used is shown in Fig. 10, where Mat₁ and Mat₂ are material B and A in Table 3, respectively, and IC1 in $\vartheta = -180^\circ$ is frictional contact and IC2 in $\vartheta = 0^\circ$ is a perfectly bonded interface condition. The friction coefficients for IC1 are indicated in Table 11 for each case in the first column³.

³ In the expression proposed by Comninou [24], it should be taken into account the following relation between $\lambda_{\text{Comninou}}$ and λ used in the present article

$$\lambda = 1 - \lambda_{\text{Comninou}} \tag{78}$$

None of the solutions obtained with $f > 0$ with the eigenequation found in [24] satisfies the frictional dissipation of energy condition. This is because the compliant material is the upper material in the interface crack corner. Therefore, to obtain results that fulfill the frictional dissipation of energy condition, one possibility is to interchange the material position obtaining the same result as if we change the sign of f , which implies changing the direction of the friction shear stress

Table 9

Example 2.4. Numerical values of the $0 < \lambda < 1$ and ω shown in Fig. 8 for open orthotropic bi-material corners with friction interface described in the figure, see Section 6.1.2. (*) Fulfills the frictional dissipation of energy condition. (o) No frictional tangential stress on the contact face, including anti-plane mode.

BC2	λ, ω					
	$\mu = 0$	$\mu = 0.2$	$\mu = 0.4$	$\mu = 0.6$	$\mu = 0.8$	$\mu = 1$
F $\vartheta_2 = 90^\circ$	0.758705740 179.772° (o)	0.684127938 165.666°	0.631431721 156.104°	0.592058527 149.660°	0.560533418 145.134°	0.533921907 141.805°
	0.758705740 -0.227° (o)	0.857890753 18.526° (*)	0.954851180 37.297° (*)	0.932644906 -58.085°	0.824276832 -75.173°	0.687979912 -91.2789°
F $\vartheta_2 = 105^\circ$	0.629233980 169.775° (o)	0.589927781 156.629°	0.562410504 148.017°	0.541586923 142.507°	0.524250842 138.767°	0.509291795 136.073° (*)
	0.629233980 -10.224° (o)	0.682597964 4.935° (*)	0.744030910 17.268° (*)	0.809888175 26.674° (*)	0.879729113 34.476°	0.953168543 41.425°
F $\vartheta_2 = 120^\circ$	0.562179580	0.544186082	0.531446795	0.521304585	0.512619999	0.504861326 129.905° (*)
	152.931° (o)	143.196°	137.577°	134.054°	131.651° (*)	0.741198610 26.243° (*)
	0.562179580	0.589646083	0.624729071	0.661993250	0.700578854	0.497342926 -102.236° (*)
F $\vartheta_2 = 135^\circ$	-27.069° (o)	-11.763° (*)	3.181° (*)	13.550° (*)	20.760° (*)	0.523575361 -90.629° (*)
	0.527596524	0.522288584	0.518236821	0.514826624	0.511801503	0.509035099 122.937° (*)
	131.541° (o)	128.035°	125.980°	124.626°	123.662° (*)	0.622167787 11.762° (*)
	0.527596524	0.535983431	0.552393349	0.575896257	0.599302798	0.484442677 -101.602° (*)
F $\vartheta_2 = 150^\circ$	-48.458° (o)	-41.335° (*)	-25.784° (*)	-7.801° (*)	4.014° (*)	0.513757233 -79.689° (*)
	0.509880836 111.755° (o)	0.511589363 112.418°	0.513129832 112.894°	0.514557475 113.256°	0.515902136 113.543°	0.517182070 113.778°
	0.509880836 -68.245° (o)	0.507891475 -69.242° (*)	0.505353001 -70.923° (*)	0.501493604 -74.276° (*)	0.494060198 -81.972° (*)	0.482004862 -94.017° (*)
F $\vartheta_2 = 165^\circ$	0.501721950 96.999° (o)	0.506768441 97.885°	0.511711793 98.687°	0.516557375 99.4236°	0.521304551 100.103°	0.525958871 100.736°
	0.501721950 -83.001° (o)	0.496566407 -83.989° (*)	0.491293648 -85.108° (*)	0.485892755 -86.392° (*)	0.480349885 -87.891° (*)	0.474649212 -89.667° (*)
F $\vartheta_2 = 180^\circ$	0.500000000 90.000° (o)	0.505971387 90.000°	0.511938575 90.000°	0.517897380 90.000°	0.523843655 90.000°	0.529773307 90.000°
	0.500000000 -90.000° (o)	0.494028613 -90.000° (*)	0.488061425 -90.000° (*)	0.482102620 -90.000° (*)	0.476156345 -90.000° (*)	0.470226693 -90.000° (*)

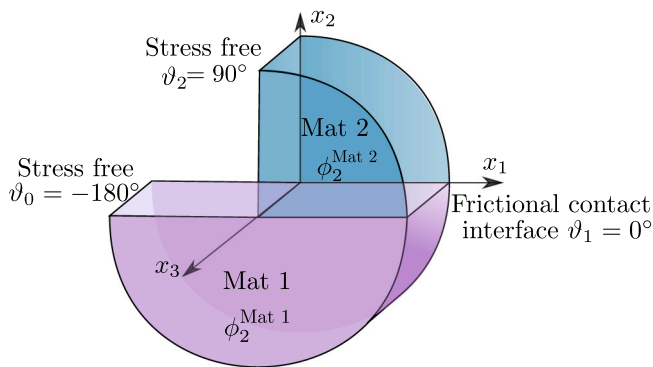


Fig. 9. Example 2.5. Schema of broken graphite/epoxy laminate as an open bi-material corner with frictional contact interface. Mat. 1 and Mat. 2 are material D in Table 3, and friction coefficient $\mu = 0.5$. Results presented in Table 10, see Section 6.1.2.

considering compressions in the contact zone. The present matrix formalism does not need to use negative friction coefficients, as it has the possibility of having a sliding angle in the opposite direction. It has also been checked that for a friction coefficient $\mu = 0$ or in the homogeneous case ($\text{Mat}_1 = \text{Mat}_2$), the combination of materials does not matter, $\lambda = 0.5$, as explained in [24,50]. The singular solutions associated with

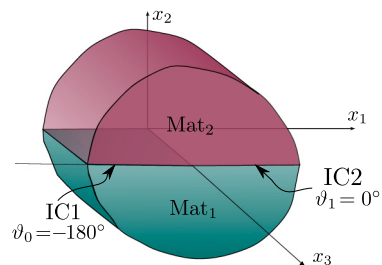


Fig. 10. Configuration used for interface crack examples.

λ_1, ω_1 and λ_3, ω_3 represent a symmetric set of nonsymmetric solutions, each one can be obtained from the other simply by multiplying it by -1 .

Example 3.2. Frictional interface crack in an anisotropic bi-material. The results by Comninou [24,50] for the contact model of interface cracks in isotropic bi-materials were later generalised to anisotropic bi-materials by many authors, see [51] for most relevant references. In Table 12, the present results are compared with those obtained by solving a closed-form eigenequation for λ derived by Sung and Chung [35]. The configuration used is as shown in Fig. 10, with

Table 10

Example 2.5. Numerical values for the singularity exponent $0 < \lambda < 1$ and sliding angle ω for two single-material wedges sliding with friction in both interfaces, see Section 6.1.2. (*) Fulfills the frictional dissipation of energy condition. Shaded cells contain results obtained with the present code that match the results obtained in [31].

$\phi_2^{\text{Mat}_2}$ \ / \ $\phi_2^{\text{Mat}_1}$	λ, ω				
	0°	30°	45°	60°	90°
-90°	0.548017099 180.000° (*)	0.565900331 159.902° (*)	0.564170398 164.051°	0.561171875 170.835°	0.560019792 180.000°
			0.936447242 -61.819°	0.934542791 -60.596°	
-60°	0.605308605 144.586°	0.611539789 143.912°	0.599601087 150.622°	0.588025012 158.476°	0.578173913 167.378°
			0.961278926 -54.322°	0.942248425 -55.138°	
-45°	0.611133541 150.646°	0.621837505 147.374°	0.613167283 153.271°	0.604286635 160.198°	0.596516326 167.626°
			0.988349267 43.524°	0.954982281 47.267°	
-30°	0.612204427 160.596°	0.627108419 152.655°	0.622137106 157.770°	0.616423552 164.162°	0.611076764 171.468°
			0.951241488 39.220°	0.921431011 42.986°	
0°	0.614714632 180.000°	0.623845018 162.622°	0.624200402 166.189°	0.623734137 171.950°	0.623688164 180.000°
		0.948633865 25.917°	0.905792839 32.618°	0.882083653 34.842°	0.932323131 0°
30°	0.612204427 -160.596°	0.598802691 170.662°	0.601648274 172.811°	0.604867872 178.793°	0.611076764 -171.468°
			0.959118988 35.345°	0.936101118 35.994°	
45°	0.611133541 -150.646°	0.57982718 172.200°	0.583005574 174.284°	0.587236716 181.292°	0.596516326 -167.626°
			0.990008663 42.775°	0.961588569 44.212°	
60°	0.605308605 -144.584°	0.582203506 150.533°	0.568687031 166.523°	0.568803269 178.723°	0.578173912 -167.378°
			0.93580465 -59.476°	0.977686008 50.512°	
			0.929115054 -58.920°		

Table 11

Example 3.1. Numerical values for the singularity exponent $0 < \lambda < 1$ and sliding angle ω for an interface crack in an isotropic corner, see Section 6.2.1. (*) Fulfills the frictional dissipation of energy condition. (o) No frictional tangential stress in the interface, including anti-plane mode.

μ	Results in [24] $f = \mu$	Results in [24] $f = -\mu$	λ_1, ω_1	λ_2, ω_2	λ_3, ω_3	λ_4, ω_4
0	0.5	0.5	0.5 -90° (o)	0.5 0°	0.5 90° (o)	0.5 180°
0.2	0.486626904	0.513373096	0.5 -90° (o)	0.513373096 0° (*)	0.5 90° (o)	0.486626904 180°
0.4	0.473300850	0.52669915	0.5 -90° (o)	0.52669915 0° (*)	0.5 90° (o)	0.473300850 180°
0.5	0.466669922	0.533330078	0.5 -90° (o)	0.533330078 0° (*)	0.5 90° (o)	0.466669922 180°
0.6	0.460067898	0.539932102	0.5 -90° (o)	0.539932102 0° (*)	0.5 90° (o)	0.460067898 180°
0.8	0.446972184	0.553027816	0.5 -90° (o)	0.553027816 0° (*)	0.5 90° (o)	0.446972184 180°
1	0.43405509	0.56594491	0.5 -90° (o)	0.56594491 0° (*)	0.5 90° (o)	0.43405509 180°

Mat₁ and Mat₂ indicated in Table 12 and the interface conditions IC1 and IC2 are frictional contact and perfectly bonded, respectively. Orthotropic materials are represented with fibres that match the x₁-axis, apparently monoclinic materials are orthotropic materials with

the fibre in x₁x₃-plane but with a ϕ_2 angle measured from the x₁-axis or with the fibre in x₁x₂-plane but with a ϕ_3 angle measured from the x₁-axis and apparently anisotropic materials are orthotropic materials whose fibre is rotated an angle ϕ_2 around the x₂-axis and

an angle ϕ_3 around the x_3 -axis, as represented in Fig. 5. Excellent agreement is found between [35] and the present results for orthotropic and apparently monoclinic materials with fibres in the x_1x_2 -plane, but no coincidence is found either in the case of monoclinic materials with fibres in the x_1x_3 -plane or in general anisotropic materials. This mismatch can be explained by analysing the frictional sliding contact model used by Sung and Chung in [35], where the angle ω , direction of the tangential stress, is not defined, assuming that the values of the frictional tangential stresses σ_{i2} with $i = 1, 3$ are either zero or $\pm\mu\sigma_{22}$. A procedure similar to that previously developed for open corners with frictional contact in [49] is applied in [51] to the frictional interface crack problem, whose results agree with those obtained by the present matrix formalism.

As was checked for the isotropic case, it was also checked for any orthotropic or monoclinic material with a PES parallel to the coordinate planes x_1x_3 or x_1x_2 , in the frictionless case with $\mu = 0$ and in the case of similar or identical materials ($\text{Mat}_1 = \text{Mat}_2$ with $\phi_1^1 = \phi_2^2$), that $\lambda = 0.5$ as well; however, in the case of dissimilar general anisotropic materials with $\mu = 0$, $\lambda = 0.5 \pm i\epsilon$. Apart from the special cases (frictionless contact, similar or identical materials, antiplane case with zero compression and zero friction shear), if we only consider the singular solutions that meet the frictional dissipation of energy criterion, then $\text{Re}(\lambda) > 0.5$. This observation is important as it shows that under friction and with dissimilar materials the singularity will be weaker than in the frictionless case or the case of similar or identical materials.

When the last example in Table 12, corresponding to a bi-material formed by a semi-plane of material G with $\varphi_2 = 60^\circ$ and a semi-plane of material E with $\varphi_2 = 30^\circ$ and $\varphi_3 = -2^\circ$ (an apparently anisotropic material), is solved with the present code, complex values are obtained for both λ and ω . Therefore, this problem is also analysed with the code currently under development for the special case of complex λ where two angles ω , ω' and ω'' , are obtained for the frictional shear vector. The treatment of complex singularity exponents λ is discussed in more detail in Section 7. For completeness, the result obtained with this code are added to this table as well.

The crack tip singularity in interface cracks with frictional contact was also studied by Leguillon [33] for isotropic and anisotropic bi-materials. In the model proposed in [33], the sliding direction is assumed as a kinematic condition and can be chosen in any direction between the plane mode and the anti-plane mode, this differs from the model considered in the present work. Thus, good agreement can only be achieved when comparing the results in [33] to those of the present study for isotropic materials and orthotropic materials with a stacking sequence of [0,90], when prescribing a sliding angle of 0° or 90° .

Example 3.3. Closed crack tip terminating at a perfectly bonded interface. Fig. 11 represents the configuration considered in the examples presented in Table 13, where the crack is located in one of the bonded materials and not on the interface. This case can be studied as a closed corner consisting of a three-material wedge, and was studied by Comninou and Dundurs [25] among many other authors. Some tests have been carried out to compare the results of the present procedure with the results obtained from eigenequation [25, Eq. (5)], all with perfect agreement. In Table 13 some of these numerical results are shown. Mat_1 and Mat_3 are material B and Mat_2 material A in Table 3. In Table 13, the angle $\theta_1 - \theta_0$ is indicated for each case. In this example, the inclination of the crack that terminates at the interface is varied by changing the angle $0 \leq \theta_0 \leq 180^\circ$, while keeping the angles $\theta_1 = 0^\circ$ and $\theta_2 = 180^\circ$ fixed. The $\theta_3 = \theta_0 + 360^\circ$ is varying together with θ_0 . The friction coefficient used at the interface IC1 is $\mu = 1$. IC2 and IC3 are perfectly bonded interfaces. In Table 13, crack inclinations for which no singularity exponent was found in the range $0 < \lambda < 1$ have been marked with the symbol $-$.

It has also been checked that:

- When $\theta_0 = 90^\circ$ in Fig. 11, the results do not depend on the friction coefficient, this is evident due to the symmetry generated in the corner geometry.

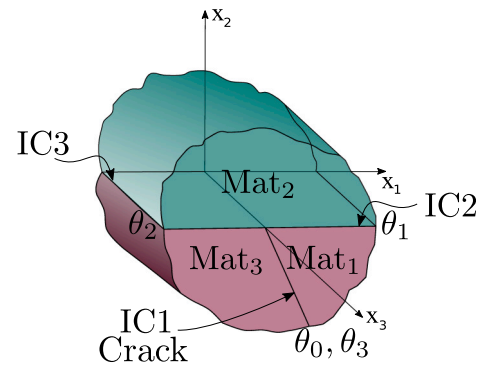


Fig. 11. Corner configuration for examples in Table 13, crack reaching a perfectly bonded interface.

- When θ_0 approaches the values 0° or 180° , in Fig. 11, the results for λ tend to the λ value in the case of a frictional interface crack.
- The singular solutions associated with λ_1, ω_1 and λ_3, ω_3 represent a symmetric set of non-symmetric solutions, each one can be obtained from the other just by multiplying it by -1 as they correspond to the anti-plane mode. These solutions are also symmetric with respect to the solutions associated with λ_1, ω_1 and λ_3, ω_3 for a problem with a crack inclination $\theta'_1 - \theta'_0 = (\theta_1 - \theta_0) - \theta_2$, which could be easily explained by symmetry arguments in view of the isotropy of the materials.

6.2.2. Singular solutions for closed corners with two single-material wedges

Example 4. Arias et al. [28] studied the case of two isotropic materials sliding one over the other with two frictional contact interfaces for the case of tectonic plates. Table 14 shows no considerable difference between the results obtained with the present matrix formalism and the results obtained with the eigenequation presented by Arias et al. [28] for isotropic homogeneous corners. The material used in the calculation is material A from Table 3, but the same results are obtained for any isotropic material, as long as the same material is chosen for both wedges. As this example has frictional contact on IC1 and IC2, both interfaces must simultaneously fulfil the compression condition. This requirement is checked and in most cases presented in Table 14 it is not met. Solutions not fulfilling the compression condition simultaneously at both interfaces are marked with (\pm) .

7. Concluding remarks

This article generalises the semi-analytic matrix formalism for singularity analysis of anisotropic linear elastic multi-material corners and the computational procedure developed in [18], covering also cases with any finite number of frictional sliding contact surfaces. It expands and completes the matrix formalism introduced in a concise way in [37,38]. The main contribution of this article is the presentation of a general implementation of the procedure that has been extensively tested and validated through numerous numerical examples. This implementation also serves to confirm the excellent accuracy and efficiency of the proposed matrix formalism.

The main features of the developed code are:

- Any finite number of single-material wedges in the corner
- Any linear elastic and homogeneous material in each wedge
- Generalised plane strain (GPS) $u_i(x, y)$, $i = x, y, z$, a kind of 2.5D elastic problem formulation
- Any finite number of frictional surfaces, outer boundary surfaces or interfaces, in the corner
- A 3D Coulomb law for isotropic friction represented by Coulomb cone.

Table 12

Example 3.2. Numerical values for the singularity exponent $0 < \lambda < 1$ and sliding angle ω for an interface crack between anisotropic materials, see Section 6.2.1. (*) Fulfills the frictional dissipation of energy condition. (o) No frictional tangential stress in the interface, including anti-plane mode.

μ	Mat ₁	Mat ₂	Results in [35]	λ_1, ω_1	λ_2, ω_2	λ_3, ω_3	λ_4, ω_4
0.5	G	E	0.501651679	0.5 (o)	0.501651679	0.5 (o)	0.498348321
			$f = 0.5$	-90°	0° (*)	90°	180°
1	$\phi_1 = 0^\circ$	$\phi_1 = 0^\circ$	0.503303268	0.5 (o)	0.503303268	0.5 (o)	0.496696732
			$f = 1$	-90°	0° (*)	90°	180°
0.5	G	E	0.502122213	0.5 (o)	0.502122213	0.5 (o)	0.496523204
			$f = 0.5$	-90°	-0° (*)	90°	180°
1	$\phi_3 = 60^\circ$	$\phi_3 = 30^\circ$	0.503552288	0.5 (o)	0.503552288	0.5 (o)	0.489789778
			$f = 1$	-90°	-0° (*)	90°	180°
0.5	G	E	0.509595142	0.5 (o)	0.511519758	0.5 (o)	0.488480242
			$f = 0.5$	237.377°	-45.007° (*)	57.377°	134.992°
1	$\phi_2 = 60^\circ$	$\phi_2 = 30^\circ$	0.519172879	0.5 (o)	0.523009419	0.5 (o)	0.476990581
			$f = 1$	237.377°	-45.007° (*)	57.377°	134.992°
1	G	E $\phi_2 = 30^\circ$	0.516405370	0.503192599	0.523049834		0.477013012
			$\phi_2 = 60$	$\phi_3 = -2^\circ$	$f = 1$	240.639°	-47.067° (*)

μ	Mat ₁	Mat ₂	λ_5, ω_5	λ_6, ω_6
0.5	G	E	0.493212664	0.506787336
			$\phi_2 = 60^\circ$	$\phi_2 = 30^\circ$
1	$\phi_2 = 60^\circ$	$\phi_2 = 30^\circ$	0.486431495	0.513568505
			$\phi_3 = -2^\circ$	$\phi_3 = -2^\circ$
1	G	E $\phi_2 = 30^\circ$	0.483420518	0.506309057 ± i0.0018419970
	$\phi_2 = 60^\circ$	$\phi_3 = -2^\circ$	-137.876°	$\omega' = 54.256^\circ, \omega'' = 50.543^\circ$

Table 13

Example 3.3. Numerical values for the singularity exponent $0 < \lambda < 1$ and sliding angle ω for a crack terminating at a perfectly bonded interface in an isotropic corner with a friction coefficient in the crack $\mu = 1$, see Section 6.2.1. (*) Fulfills the frictional dissipation of energy condition. (o) No frictional tangential stress in the interface, including anti-plane mode.

$\theta_1 - \theta_0$	Results in [25]	λ_1, ω_1	λ_2, ω_2	λ_3, ω_3	λ_4, ω_4
0°	0.43405509	0.5 -90° (o)	0.43405509 0°	0.5 90° (o)	0.56594491 180° (*)
15°	0.508410685	0.543314279 -90° (o)	0.508410685 0°	0.543314279 90° (o)	0.639143816 180° (*)
30°	0.633740388	0.594708947 -90° (o)	0.633740388 0°	0.594708947 90° (o)	0.683933616 180° (*)
45°	-	0.656319424 -90° (o)	- -	0.656319424 90° (o)	0.669427348 180°
60°	-	0.730292305 -90° (o)	- -	0.730292305 90° (o)	0.6347699 180°
75°	0.822212612	0.814682253 -90° (o)	0.822212612 0° (*)	0.814682253 90° (o)	0.62589152 180°
90°	0.6633562	0.869773695 -90° (o)	0.663356243 0° (o)	0.869773695 90° (o)	0.663356243 180° (o)
105°	0.62589152	0.814682253 -90° (o)	0.62589152 0°	0.814682253 90° (o)	0.822212612 180° (*)
120°	0.6347699	0.730292305 -90° (o)	0.6347699 0°	0.730292305 90° (o)	-
135°	0.669427348	0.656319424 -90° (o)	0.669427348 0°	0.656319424 90° (o)	-
150°	0.683933616	0.594708947 -90° (o)	0.683933616 0° (*)	0.594708947 90° (o)	0.633740388 180°
165°	0.639143816	0.543314279 -90° (o)	0.639143816 0° (*)	0.543314279 90° (o)	0.508410685 180°
180°	0.56594491	0.5 -90° (o)	0.56594491 0° (*)	0.5 90° (o)	0.43405509 180°

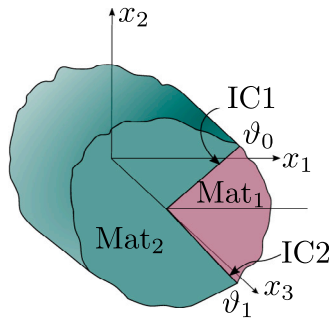
- Collinearity of friction shear vector and the relative displacement vector is satisfied.
- The frictional dissipation of the energy condition and compression condition are checked.

An excellent accuracy and robustness of the code, due to its semi-analytic character, is confirmed by the agreement of the results of the present code, up to a high number of digits coinciding, with the numerical solutions of corner-singularity eigenequations deduced by

Table 14

Example 4. Numerical values for the singularity exponent $0 < \lambda < 1$ and sliding angle ω for two isotropic single-material wedges sliding with friction in both interfaces, see Section 6.2.2. In [28], a friction coefficient on one face is denoted as f , and a specific ratio of the friction coefficients on both faces as w . (*) Fulfills the frictional dissipation of energy condition. (o) No frictional tangential stress in the interface, including anti-plane mode. (\pm) One contact interface under compression and the other contact interface under tension.

Corner configuration	IC1	IC2	Results λ in [28]	Present results $\lambda, \omega_1, \omega_2$
			0.349057987	0.349057987
			$f = 0.4, w = 1$	$\omega_0 = \omega_1 = 0^\circ$
			0.726220223	0.726220223 (\pm)
			$f = 0.4, w = 1$	$\omega_0 = \omega_1 = 0^\circ$
			0.734403364	0.734403364 (\pm)
			$f = -0.4, w = -1$	$\omega_0 = 180^\circ, \omega_1 = 0^\circ$
			0.147909364	0.147909364
			$f = -0.4, w = -1$	$\omega_0 = 180^\circ, \omega_1 = 0^\circ$
	$\mu = 0.4$	$\mu = 0.4$	0.410676802	0.410676802 (*)
	$\vartheta_0 = 30^\circ$	$\vartheta_1 = 330^\circ$	$f = 0.4, w = -1$	$\omega_0 = 0^\circ, \omega_1 = 180^\circ$
			0.704192317	0.704192317 (\pm)
			$f = 0.4, w = -1$	$\omega_0 = 0^\circ, \omega_1 = 180^\circ$
			0.349057987	0.349057987
			$f = -0.4, w = 1$	$\omega_0 = \omega_1 = 180^\circ$
			0.726220223	0.726220223 (\pm)
			$f = -0.4, w = 1$	$\omega_0 = \omega_1 = 180^\circ$
			-	0.6 (o)
				$\omega_0 = \omega_1 = \pm 90^\circ$
			0.351115240	0.351115240
			$f = -1, w = 0.5$	$\omega_0 = \omega_1 = 0^\circ$
			0.731708957	0.731708955 (\pm)
			$f = -1, w = 0.5$	$\omega_0 = \omega_1 = 0^\circ$
			0.737966428	0.737966428 (\pm)
			$f = -1, w = -0.5$	$\omega_0 = 180^\circ, \omega_1 = 0^\circ$
			0.513337305	0.513337355 (\pm)
			$f = 1, w = -0.5$	$\omega_0 = 0^\circ, \omega_1 = 180^\circ$
	$\mu = 0.5$	$\mu = 1$	0.600884868	0.600884868 (\pm)
	$\vartheta_0 = 30^\circ$	$\vartheta_1 = 330^\circ$	$f = 1, w = -0.5$	$\omega_0 = 0^\circ, \omega_1 = 180^\circ$
			0.890144750	0.890144750 (\pm)
			$f = 1, w = -0.5$	$\omega_0 = 0^\circ, \omega_1 = 180^\circ$
			0.511522494	0.511522501 (\pm)
			$f = 1, w = 0.5$	$\omega_0 = \omega_1 = 180^\circ$
			0.712545420	0.712545420 (\pm)
			$f = 1, w = 0.5$	$\omega_0 = \omega_1 = 180^\circ$
			-	0.6 (o)
				$\omega_0 = \omega_1 = \pm 90^\circ$



other authors for some specific and relevant engineering problems. Actually, the present solutions not only cover the solutions of the specific eigenequations, but often singular solutions not detected by solving the specific eigenequations are found, due to considering GPS states instead of plane (2D) elastic states often considered in the deduction of specific eigenequations. Although the present procedure works for any finite number of frictional contact faces $F \geq 0$, only cases with $F = 1$ and $F = 2$ found in literature are studied in the present article for the testing purposes.

Advantages of the present code. As previously mentioned in [18], there are several benefits and positive aspects associated with the use of the developed code, which include the following:

- One of the key advantages of this code is its versatility. It is capable of solving a wide range of problems with a variety of boundary and interface conditions, including any finite number of frictional contact surfaces, as well as any linear elastic material properties. This makes it a highly useful tool for addressing a multitude of stress singularity problems.
- The code developed in this work exhibits a high degree of accuracy and reliability. A comparison of the numerical results computed by this code with those obtained from the numerical solution of closed-form eigenequations found in the literature reveals that they are essentially identical, up to at least 8 digits.

This exceptional level of accuracy is due to the semi-analytic nature of the procedure, which employs numerical algorithms to find the roots of the sextic Lekhnitskii–Stroh characteristic polynomial for anisotropic materials when a solution in radicals is not possible [52], and to find the roots of the transcendental eigenequation for the corner problem. The remainder of the calculations are performed analytically, providing maximum accuracy. In fact, using modern computer algebra software to work with numbers stored at arbitrarily high precision, it is possible to achieve an arbitrary level of accuracy.

- This code is user-friendly and easily expandable due to its modular design. This is demonstrated in this paper, since starting from the developed code presented in [18], this article details in Section 5 the changes made in the code to add the possibility of solving problems with frictional contact.
- In addition to the potential self-checks mentioned in [18], the inclusion of the interface and boundary frictional contact condition options in the code opens up the possibility for additional self-checks to be performed.
 - The frictionless interface case can be studied using the frictionless interface condition or applying a friction coefficient $\mu = 0$. The size of the matrices and the solution method of the characteristic system are different, but the results obtained for λ and $w(r, \vartheta)$ are the same.

- When applying a friction coefficient $\mu = 0$ to a boundary and when applying the symmetry boundary condition (only u_θ restricted), despite having different sizes of the characteristic matrix, the results are the same in both cases.
- In the present formalism, the use of $\mu < 0$ is not intended. However, it has been used for verification purposes. The problem is first solved using the friction coefficient $\mu > 0$. If λ_1, ω_1 is a solution to the problem, then when solving it again with the friction coefficient $-\mu$, the solution should be λ_1, ω_2 , where $\omega_2 = \omega_1 + \pi$.

This kind of new self-check is useful to ensure the accuracy and reliability of the code results, especially when including new features and implementations on different computer platforms.

Complex singularity exponent $\lambda \in \mathbb{C}$ in presence of frictional contact. As shown in the numerical results, in cases of frictional contact between isotropic materials, or orthotropic materials with a PES $x_3 = 0$, potentially valid solutions with $\lambda \in \mathbb{C}$ and $\omega \in \mathbb{R}$ may appear. In the case of frictionless contact on one face of an anisotropic material and complex $\lambda \in \mathbb{C}$, it was observed by studying the solution in displacements that there are two different relative sliding angles ω'_u and ω''_u on the surface in contact. Assuming a continuous variation of the friction coefficient from zero to positive values, it is considered that the values of ω'_u, ω''_u and λ vary continuously. Therefore, another procedure is needed for modelling the frictional contact, which considers a complex λ and two values of ω'_u and ω''_u as unknowns on each frictional surface. These cases of complex λ are not covered in the present work for the sake of brevity. However, by taking advantage of one of the benefits of code, which is its ability to be expanded, the code has recently been generalised to allow solutions of problems with frictional contact and complex singularity exponent $\lambda \in \mathbb{C}$. This new procedure, which considers two angles, ω' and ω'' , of frictional shear vector for a $\lambda \in \mathbb{C}$ has already been implemented and tested, and will be presented in a forthcoming work, for the sake of simplicity and brevity. In the present article, the generalised code for complex singularity exponents is used in Example 3.2 in Table 12 as noted above.

The existence of $\lambda \in \mathbb{C}$ solution entails oscillatory stress fields, which involve an infinite number of compression and tension zones that interchange with each other in the contact zone near the corner apex, thus not meeting the compression condition. To give a physical meaning and utility to a complex singular eigensolution with $\lambda \in \mathbb{C}$ either for frictional or frictionless contact, we propose the concept of *small scale tension zone*, where the distance from the corner apex to the far end of the tension zone that is located farthest from the corner vertex is much smaller than the relevant characteristic length of the boundary value problem under study.

Anisotropic frictional contact. The theoretical formulation of the matrix formalism introduced in [37,38] also considers anisotropic friction, which means that the sliding direction and the frictional shear direction can be different, and then as a result the friction coefficient μ varies as a function of these directions [20,53,54]. The computational implementation of this theoretical formulation in the present code is quite straightforward, and it would allow characterising stress singularities in the configurations where this direction-dependent friction anisotropy is relevant.

Power-logarithmic stress singularities. It can be expected that the semi-analytic nature of the present procedure will allow a generalisation to also cover power-logarithmic stress singularities following the strategy in complex variable developed in [17], but the need to include the angles ω_{k_i} among the unknowns will require some modifications of the strategy in [17].

CRediT authorship contribution statement

María A. Herrera-Garrido: Software, Validation, Visualization, Writing – original draft. **Vladislav Mantić:** Conceptualization, Validation, Writing – review & editing, Supervision, Funding acquisition. **Alberto Barroso:** Writing – review & editing, Supervision, Funding acquisition.

Declaration of competing interest

The authors declare that they have no known competing financial interests or personal relationships that could have appeared to influence the work reported in this paper.

Data availability

The data used are available in the literature. The online application based on the code presented will be available for use by other researchers.

Acknowledgements

The authors acknowledge that the code presented in this work is based on the code developed by Ing. Jara Allo, MSc in her Master's Thesis [55]. The research was carried out with the support of the Spanish Ministry of Science, Innovation, and Universities. PID2021-123325OB-I00, PGC2018-099197-B-I00; Consejería de Transformación Económica, Industria, Conocimiento y Universidades, Junta de Andalucía: P18-FR-1928, US-1266016; European Regional Development Fund: PID2021-123325OB-I00, PGC2018-099197-B-I00, P18-FR-1928, US-1266016.

Appendix A. Basic relations of the Stroh formalism applied for the stress singularity analysis

A brief explanation of the Stroh formalism [39–42] used to describe the power-law singular elastic solutions in linearly elastic anisotropic materials is given below.

From the linear elastic constitutive equation

$$\sigma_{ij} = C_{ijkl}\epsilon_{kl} = C_{ijkl}u_{k,l}, \quad (\text{A.1})$$

relating stresses σ_{ij} , small strains ϵ_{ij} , and displacements u_i , with $i, j = 1, 2, 3$, and under the assumption of generalised plane strain (GPS) conditions, the following equilibrium equation, in the absence of body forces, is obtained

$$C_{ijkl}u_{k,lj}(x_1, x_2) = 0, \quad (\text{A.2})$$

which is a second order elliptic system of three partial differential equations (PDEs). Then, a solution of (A.2) given as a function

$$u_k(x_1, x_2) = a_k f(z), \quad (\text{A.3})$$

of a complex variable

$$z = x_1 + px_2. \quad (\text{A.4})$$

is considered. By differentiating twice (A.3) and substituting in (A.2), the following quadratic eigenvalue problem is obtained

$$[C_{i1k1} + p(C_{i1k2} + C_{i2k1}) + p^2 C_{i2k2}]a_k = 0, \quad (\text{A.5})$$

where a_k is a complex vector and p is a complex constant, both to be determined. Defining the matrices

$$Q_{ik} = C_{i1k1}, \quad R_{ik} = C_{i1k2}, \quad T_{ik} = C_{i2k2}, \quad (\text{A.6})$$

the eigenvalue problem (A.5) can be written in matrix form as

$$[\mathbf{Q} + p(\mathbf{R} + \mathbf{R}^T) + p^2 \mathbf{T}]\mathbf{a} = \mathbf{0}. \quad (\text{A.7})$$

To solve this eigenvalue problem, first the roots of the matrix determinant are found,

$$\det(\mathbf{Q} + p(\mathbf{R} + \mathbf{R}^T) + p^2\mathbf{T}) = 0. \quad (\text{A.8})$$

This is a polynomial equation of sixth degree in p with real coefficients, whose solution are three pairs of conjugate complex roots called eigenvalues,

$$\text{Im } p_\alpha > 0, \quad p_{\alpha+3} = \bar{p}_\alpha, \quad \alpha = 1, 2, 3 \quad (\text{A.9})$$

The eigenvectors associated to p_α are denoted as \mathbf{a}_α .

For stresses, the stress function vector $\boldsymbol{\varphi}_i$ is introduced,

$$\boldsymbol{\varphi}_i(z) = b_i f(z) \quad \text{or in matrix notation} \quad \boldsymbol{\varphi} = \mathbf{b}f(z). \quad (\text{A.10})$$

The vector \mathbf{b} is related to the vector \mathbf{a} through the matrices \mathbf{Q} , \mathbf{R} and \mathbf{T} and the eigenvalue p as

$$\mathbf{b}_\alpha = (\mathbf{R}^T + p_\alpha \mathbf{T})\mathbf{a}_\alpha = -\frac{1}{p_\alpha}(\mathbf{Q} + p_\alpha \mathbf{R})\mathbf{a}_\alpha. \quad (\text{A.11})$$

As there are three pairs of complex roots p_α , there are also three pairs of eigenvectors \mathbf{a}_α and \mathbf{b}_α ,

$$\mathbf{a}_{\alpha+3} = \bar{\mathbf{a}}_\alpha \quad \text{and} \quad \mathbf{b}_{\alpha+3} = \bar{\mathbf{b}}_\alpha, \quad \alpha = 1, 2, 3. \quad (\text{A.12})$$

For the analysis of the stress singularities, following general mathematical results for elliptic PDEs by [56,57], the power-law singularities in the form $f_\alpha(z_\alpha) = z_\alpha^\lambda q_\alpha$ are considered, for the sake of simplicity. This leads to

$$f_\alpha(z_\alpha) = z_\alpha^\lambda q_\alpha, \quad f_{\alpha+3}(\bar{z}_\alpha) = \bar{z}_\alpha^\lambda \bar{q}_\alpha, \quad (\text{A.13})$$

where q_α and \bar{q}_α are constants and λ is the characteristic singularity exponent.

Using the relations between the Cartesian and polar coordinates, $x_1 = r \cos(\theta)$ and $x_2 = r \sin(\theta)$, the complex variable z in (A.4) can be expressed as a function of r and θ . This will make it easier to deal with expressions for the geometry of the corner problem, see Fig. 1,

$$z_\alpha = r(\cos(\theta) + p_\alpha \sin(\theta)) = r\zeta_\alpha^\lambda(\theta). \quad (\text{A.14})$$

Introducing now a suitable notation for a diagonal matrix as

$$\langle z_\alpha^\lambda \rangle = \text{diag}(z_1^\lambda, z_2^\lambda, z_3^\lambda), \quad (\text{A.15})$$

and substituting (A.14) into (A.15), we get

$$\langle z_\alpha^\lambda \rangle = r^\lambda \text{diag}(\zeta_1^\lambda(\theta), \zeta_2^\lambda(\theta), \zeta_3^\lambda(\theta)) = r^\lambda \langle \zeta_\alpha^\lambda(\theta) \rangle. \quad (\text{A.16})$$

The 3×3 complex square matrices \mathbf{A} and \mathbf{B} are defined by the three eigenvectors \mathbf{a}_α and \mathbf{b}_α , respectively, as column vectors,

$$\mathbf{A} = [\mathbf{a}_1, \mathbf{a}_2, \mathbf{a}_3], \quad \mathbf{B} = [\mathbf{b}_1, \mathbf{b}_2, \mathbf{b}_3]. \quad (\text{A.17})$$

By substituting \mathbf{A} and \mathbf{B} , together with the expressions (A.13) and (A.16) in (A.3) and in (A.10), the general expressions for the power-law displacement and stress function vectors $\mathbf{u}(r, \theta)$ in (1) and $\boldsymbol{\varphi}(r, \theta)$ (2) are obtained. These two vectors can be arranged as the 6×1 vector of elastic variables as

$$\mathbf{w}(r, \theta) = \begin{bmatrix} \mathbf{u}(r, \theta) \\ \boldsymbol{\varphi}(r, \theta) \end{bmatrix} = r^\lambda \mathbf{XZ}^\lambda(\theta)\mathbf{t}, \quad (\text{A.18})$$

where

$$\mathbf{X} = \begin{bmatrix} \mathbf{A} & \bar{\mathbf{A}} \\ \mathbf{B} & \bar{\mathbf{B}} \end{bmatrix}, \quad \mathbf{t} = \begin{bmatrix} \mathbf{q} \\ \bar{\mathbf{q}} \end{bmatrix}, \quad \mathbf{Z}^\lambda(\theta) = \begin{bmatrix} \langle \zeta_\alpha^\lambda(\theta) \rangle & \mathbf{0} \\ \mathbf{0} & \langle \bar{\zeta}_\alpha^\lambda(\theta) \rangle \end{bmatrix}. \quad (\text{A.19})$$

For the sake of brevity, the theoretical formulation in the present work is deduced for mathematically non-degenerate materials in the framework of the Stroh formalism. Nevertheless, this formulation can be easily generalised to degenerate and extraordinary-degenerate materials, as shown in [13,37,38]. Moreover, numerical results for some examples of degenerate materials are presented in Section 6.

Appendix B. Use of reference frames for boundary conditions of frictional contact

In this appendix, the definition of the auxiliary reference frames (11) and (12) and the boundary condition matrices in Table 1 are described in more detail based on expressions in Section 3.2.

From the Signorini condition of non-penetration in terms of the cylindrical components of displacements (18)

$$u_\theta(r, \vartheta_w) = 0, \quad (\text{B.1})$$

the following condition in terms of the Cartesian components of displacement is obtained

$$-\sin(\vartheta_w)u_1(r, \vartheta_w) + \cos(\vartheta_w)u_2(r, \vartheta_w) = 0 \quad (\text{B.2})$$

which adopts the following vector form

$$\mathbf{n}^T(\vartheta_w)\mathbf{u}(r, \vartheta_w) = 0. \quad (\text{B.3})$$

To impose the Coulomb friction law (19), first the tangential stress vector $\boldsymbol{\tau}$ is expressed by its components $\sigma_{\theta r}$ and $\sigma_{\theta 3}$ and the direction of friction shear and sliding ω as

$$|\boldsymbol{\tau}(r, \vartheta_w)| = \cos(\omega_k)\sigma_{\theta r}(r, \vartheta_w) - \sin(\omega_k)\sigma_{\theta 3}(r, \vartheta_w) = -\mu_k\sigma_{\theta\theta}(r, \vartheta_w), \quad (\text{B.4})$$

then expressing the stress components in terms of the stress function $\boldsymbol{\varphi}(r, \vartheta_w)$ as discussed in Section 3.3, and the relation of component of the stress tensor and stress function $\boldsymbol{\varphi}(r, \vartheta_w)$ [18, Eq. (98)], the condition (B.4) can be written as

$$\cos(\omega_k)\mathbf{s}_r(\vartheta_w)\boldsymbol{\varphi}_{,r}(r, \vartheta_w) + \sin(\omega_k)\mathbf{s}_3(\vartheta_w)\boldsymbol{\varphi}_{,r}(r, \vartheta_w) = \mu_k\mathbf{n}(\vartheta_w)\boldsymbol{\varphi}_{,r}(r, \vartheta_w), \quad (\text{B.5})$$

and by integrating Eq. (B.5) with respect to r and taking into account that $\boldsymbol{\varphi}(r = 0, \vartheta_w) = \mathbf{0}$ as

$$\cos(\omega_k)\mathbf{s}_r(\vartheta_w)\boldsymbol{\varphi}(r, \vartheta_w) + \sin(\omega_k)\mathbf{s}_3(\vartheta_w)\boldsymbol{\varphi}(r, \vartheta_w) = \mu_k\mathbf{n}(\vartheta_w)\boldsymbol{\varphi}(r, \vartheta_w), \quad (\text{B.6})$$

$$(\cos(\omega_k)\mathbf{s}_r(\vartheta_w) + \sin(\omega_k)\mathbf{s}_3(\vartheta_w) - \mu_k\mathbf{n}(\vartheta_w))\boldsymbol{\varphi}(r, \vartheta_w) = 0. \quad (\text{B.7})$$

By using the auxiliary vector $\mathbf{k}(\vartheta_w, \omega_k)$ (13), this expression can be rewritten as

$$(\mathbf{k}(\vartheta_w, \omega_k) - \mu_k\mathbf{n}(\vartheta_w))\boldsymbol{\varphi}(r, \vartheta_w) = 0, \quad (\text{B.8})$$

resulting in the following condition using the unit vector \mathbf{s}_μ (16)

$$\mathbf{s}_\mu(\vartheta_w, \omega_k, \mu_k)\boldsymbol{\varphi}(r, \vartheta_w) = 0. \quad (\text{B.9})$$

To ensure the condition (21), the collinearity between the relative tangential displacement and the tangential stress vectors, vector $\mathbf{m}(\vartheta_w, \omega)$ (14), perpendicular to $\mathbf{k}(\vartheta_w, \omega)$ (13), is used as an auxiliary vector. To ensure the perpendicularity of the vectors \mathbf{u} and $\boldsymbol{\tau}$ with $\mathbf{m}(\vartheta_w, \omega)$, the following relations are imposed

$$\begin{aligned} \mathbf{m}(r, \vartheta_w) \cdot \mathbf{u}(r, \vartheta_w) &= 0, \\ \mathbf{m}(r, \vartheta_w) \cdot \boldsymbol{\tau}(r, \vartheta_w) &= 0. \end{aligned} \quad (\text{B.10})$$

In view of the following identities $\mathbf{m}(r, \vartheta_w) \cdot \boldsymbol{\tau}(r, \vartheta_w) = \mathbf{m}(r, \vartheta_w) \cdot \mathbf{t}^n(r, \vartheta_w) = \mathbf{m}(r, \vartheta_w) \cdot \boldsymbol{\varphi}_{,r}(r, \vartheta_w)$, after integration with respect to r , Eq. (B.10)₂ is equivalent to

$$\mathbf{m}(r, \vartheta_w) \cdot \boldsymbol{\varphi}(r, \vartheta_w) = 0. \quad (\text{B.11})$$

From expression (B.3) and (B.10)₁, the auxiliary vectors that multiply the vector \mathbf{u} are chosen to build the matrix $\mathbf{D}_u(\vartheta_w)$ in Table 1. The matrix $\mathbf{D}_\varphi(\vartheta_w)$ in Table 1 is assembled with the auxiliary vectors that multiply the vector $\boldsymbol{\varphi}$ in (B.9) and (B.11). These four expressions will correspond to the prescribed zero values of the 4×1 vector $\mathbf{w}_{\text{corner-P}}$.

We consider 2 reference frames defined in (11) and (12), $(\mathbf{k}(\vartheta, \omega), \mathbf{m}(\vartheta, \omega), \mathbf{n}(\vartheta))$ for displacement vector and $(\mathbf{n}_\mu(\vartheta, \omega, \mu), \mathbf{s}_\mu(\vartheta, \omega, \mu), \mathbf{m}(\vartheta, \omega))$ for traction vector. The unitary vector $\mathbf{n}_\mu(\vartheta, \omega, \mu)$ is defined in the way

that it is orthogonal to $\mathbf{m}(\vartheta, \omega)$ and $\mathbf{s}_\mu(\vartheta, \omega, \mu)$. In the above, we have imposed that two components of the displacement and traction vectors in these reference frames are zero, (B.3), (B.10)₁, (B.9) and (B.11) respectively, and there is an unknown component of the displacement and traction vectors, corresponding to the $\mathbf{k}(\vartheta, \omega)$ and $\mathbf{n}_\mu(\vartheta, \omega, \mu)$ directions, respectively. In this sense, two additional expressions are needed to define the unknown variables in $\mathbf{w}_{\text{corner}_U}$,

$$u_k = ? \quad \text{and} \quad \varphi_{n_\mu} = ? \quad (\text{B.12})$$

These unknowns are obtained by multiplying $\mathbf{u}(r, \vartheta_w)$ by the matrix $\hat{\mathbf{D}}_u(\vartheta_w)$ in Table 1 and by multiplying $\boldsymbol{\varphi}(r, \vartheta_w)$ by $\hat{\mathbf{D}}_\varphi(\vartheta_w)$ also in Table 1, respectively.

Appendix C. Use of reference frames for interface conditions of frictional contact

In this appendix, the definition of the interface condition matrices is described by applying the reference frames to the expressions in Section 3.4. The Signorini condition of non-penetrability in the cylindrical components of displacements (34)

$$u_\theta^w(r, \vartheta_w) - u_\theta^{w+1}(r, \vartheta_w) = 0 \quad (\text{C.1})$$

can be written in vector form as

$$\mathbf{n}^T(\vartheta_w) \mathbf{u}^w(r, \vartheta_w) - \mathbf{n}^T(\vartheta_w) \mathbf{u}^{w+1}(r, \vartheta_w) = 0. \quad (\text{C.2})$$

Then, as matrices in (41) involve the displacement and the stress function vectors, $\mathbf{0}_{1 \times 3}$ vectors are added to multiply the components of the vectors \mathbf{w}_w and \mathbf{w}_{w+1} given by the stress function vectors, leading to

$$-\mathbf{n}^T(\vartheta_w) \mathbf{u}^w(r, \vartheta_w) + \mathbf{0}_{1 \times 3} \boldsymbol{\varphi}^w(r, \vartheta_w) - \mathbf{n}^T(\vartheta_w) \mathbf{u}^{w+1}(r, \vartheta_w) + \mathbf{0}_{1 \times 3} \boldsymbol{\varphi}^{w+1}(r, \vartheta_w) = 0. \quad (\text{C.3})$$

Expression (C.3) can be rewritten in matrix form as

$$\begin{bmatrix} -\mathbf{n}^T(\vartheta_w) & \mathbf{0}_{1 \times 3} & \mathbf{n}^T(\vartheta_w) & \mathbf{0}_{1 \times 3} \end{bmatrix} \begin{bmatrix} \mathbf{u}^w(r, \vartheta_w) \\ \boldsymbol{\varphi}^w(r, \vartheta_w) \\ \mathbf{u}^{w+1}(r, \vartheta_w) \\ \boldsymbol{\varphi}^{w+1}(r, \vartheta_w) \end{bmatrix} = 0. \quad (\text{C.4})$$

As the traction components have the same value at both sides of the interface, for the sake of symmetry, we use the sum of these values to impose the Coulomb law at both sides of the interface

$$|\tau^w(r, \vartheta_w)| + \mu_k \sigma_{\theta\theta}^w(r, \vartheta_w) + |\tau^{w+1}(r, \vartheta_w)| + \mu_k \sigma_{\theta\theta}^{w+1}(r, \vartheta_w) = 0. \quad (\text{C.5})$$

Similarly as in (B.4)–(B.7), (C.5) can be expressed in terms of the stress function vector $\boldsymbol{\varphi}(r, \vartheta_w)$ as

$$\begin{aligned} & (\cos(\omega_k) \mathbf{s}_r^T(\vartheta_w) + \sin(\omega_k) \mathbf{s}_3^T(\vartheta_w) - \mu_k \mathbf{n}^T(\vartheta_w)) \boldsymbol{\varphi}^w(r, \vartheta_w) \\ & + (\cos(\omega_k) \mathbf{s}_r^T(\vartheta_w) + \sin(\omega_k) \mathbf{s}_3^T(\vartheta_w) - \mu_k \mathbf{n}^T(\vartheta_w)) \boldsymbol{\varphi}^{w+1}(r, \vartheta_w) = 0. \end{aligned} \quad (\text{C.6})$$

Adding the corresponding $\mathbf{0}_{1 \times 3}$ vectors that multiply the displacement components of the vectors \mathbf{w}_w and \mathbf{w}_{w+1} gives

$$\begin{aligned} & \mathbf{0}_{1 \times 3} \mathbf{u}^w(r, \vartheta_w) + (\mathbf{k}^T(\vartheta_w, \omega_k) - \mu_k \mathbf{n}^T(\vartheta_w)) \boldsymbol{\varphi}^w(r, \vartheta_w) \\ & + \mathbf{0}_{1 \times 3} \mathbf{u}^{w+1}(r, \vartheta_w) + (\mathbf{k}^T(\vartheta_w, \omega_k) - \mu_k \mathbf{n}^T(\vartheta_w)) \boldsymbol{\varphi}^{w+1}(r, \vartheta_w) = 0. \end{aligned} \quad (\text{C.7})$$

Finally, using the unit vector \mathbf{s}_μ^T (16), (C.7) writes in matrix form as

$$\begin{bmatrix} \mathbf{0}_{1 \times 3} & \mathbf{s}_\mu^T & \mathbf{0}_{1 \times 3} & \mathbf{s}_\mu^T \end{bmatrix} \begin{bmatrix} \mathbf{u}^w(r, \vartheta_w) \\ \boldsymbol{\varphi}^w(r, \vartheta_w) \\ \mathbf{u}^{w+1}(r, \vartheta_w) \\ \boldsymbol{\varphi}^{w+1}(r, \vartheta_w) \end{bmatrix} = 0. \quad (\text{C.8})$$

Due to the imposed contact between both materials, the stresses must fulfil the continuity condition (equilibrium of tractions) and, therefore, the following relations

$$\sigma_{\theta j}^w(r, \vartheta_w) - \sigma_{\theta j}^{w+1}(r, \vartheta_w) = 0, \quad (\text{C.9})$$

with $j = \theta, r$, and 3. Similarly as above, the condition (C.9) can be written in terms of the stress function vector $\boldsymbol{\varphi}(r, \vartheta_w)$ as

$$\boldsymbol{\varphi}^w(r, \vartheta_w) - \boldsymbol{\varphi}^{w+1}(r, \vartheta_w) = 0. \quad (\text{C.10})$$

By adding the matrices $\mathbf{0}_{3 \times 3}$, the simultaneous fulfilment of the three equations gives

$$\mathbf{0}_{3 \times 3} \mathbf{u}^w(r, \vartheta_w) - \mathbf{I}_{3 \times 3} \boldsymbol{\varphi}^w(r, \vartheta_w) + \mathbf{0}_{3 \times 3} \mathbf{u}^{w+1}(r, \vartheta_w) + \mathbf{I}_{3 \times 3} \boldsymbol{\varphi}^{w+1}(r, \vartheta_w) = \mathbf{0}_{3 \times 1}, \quad (\text{C.11})$$

and in matrix form

$$\begin{bmatrix} \mathbf{0}_{3 \times 3} & -\mathbf{I}_{3 \times 3} & \mathbf{0}_{3 \times 3} & \mathbf{I}_{3 \times 3} \end{bmatrix} \begin{bmatrix} \mathbf{u}^w(r, \vartheta_w) \\ \boldsymbol{\varphi}^w(r, \vartheta_w) \\ \mathbf{u}^{w+1}(r, \vartheta_w) \\ \boldsymbol{\varphi}^{w+1}(r, \vartheta_w) \end{bmatrix} = \mathbf{0}_{3 \times 1}. \quad (\text{C.12})$$

The collinearity condition between the relative tangential displacement and the tangential stress vectors (38) can be imposed by verifying that both tangential vectors are perpendicular to the auxiliary vector $\mathbf{m}(r, \vartheta_w)$ (14), similar to the previous section, giving

$$\mathbf{m}(r, \vartheta_w) \cdot \Delta \mathbf{u}(r, \vartheta_w) = 0, \quad (\text{C.13})$$

with $\Delta \mathbf{u}(r, \vartheta_w) = \mathbf{u}^w(r, \vartheta_w) - \mathbf{u}^{w+1}(r, \vartheta_w)$ for the relative displacements, which in matrix form writes as

$$\begin{bmatrix} -\mathbf{m}^T(\vartheta_w, \omega_k) & \mathbf{0}_{1 \times 3} & \mathbf{m}^T(\vartheta_w, \omega_k) & \mathbf{0}_{1 \times 3} \end{bmatrix} \begin{bmatrix} \mathbf{u}^w(r, \vartheta_w) \\ \boldsymbol{\varphi}^w(r, \vartheta_w) \\ \mathbf{u}^{w+1}(r, \vartheta_w) \\ \boldsymbol{\varphi}^{w+1}(r, \vartheta_w) \end{bmatrix} = 0, \quad (\text{C.14})$$

and for the tangential stress vector

$$\mathbf{m}(r, \vartheta_w) \cdot \boldsymbol{\tau}(r, \vartheta_w) = 0. \quad (\text{C.15})$$

As before, taking into account that the stress components have the same values at both sides of the contact interface, for the sake of symmetry, we use the sum of these values to impose the collinearity of the tangential stress vector with the tangential relative displacement vector. Then, in matrix form, the condition (C.15) remains as

$$\begin{bmatrix} \mathbf{0}_{1 \times 3} & \mathbf{m}^T(\vartheta_w, \omega_k) & \mathbf{0}_{1 \times 3} & \mathbf{m}^T(\vartheta_w, \omega_k) \end{bmatrix} \begin{bmatrix} \mathbf{u}^w(r, \vartheta_w) \\ \boldsymbol{\varphi}^w(r, \vartheta_w) \\ \mathbf{u}^{w+1}(r, \vartheta_w) \\ \boldsymbol{\varphi}^{w+1}(r, \vartheta_w) \end{bmatrix} = 0. \quad (\text{C.16})$$

Collecting all expressions (C.4), (C.8), (C.12), (C.14) and (C.16) we have seven prescribed equations schematically summarised as

$$\begin{aligned} & 1 \text{ equation } \Delta u_n = 0, \\ & 1 \text{ equation } \sum \varphi_{s_\mu} = 0, \\ & 3 \text{ equations } \Delta \boldsymbol{\varphi} = 0, \\ & 1 \text{ equation } \Delta u_m = 0, \\ & 1 \text{ equation } \sum \varphi_m = 0. \end{aligned} \quad (\text{C.17})$$

These expressions, multiplied by a factor $\frac{1}{\sqrt{2}}$ to ensure orthonormality, results in the matrices \mathbf{D}_1 and \mathbf{D}_2 in Table 2. Now we can apply the following five expressions to define the unknown variables that form $\mathbf{w}_U(r, \vartheta_w)$ similarly as in (B.12)

$$\begin{aligned} & \sum u_n = ?, \\ & \sum \varphi_{n_\mu} = ?, \\ & \Delta u_k = ?, \\ & \sum u_k = ?, \\ & \sum u_m = ?. \end{aligned} \quad (\text{C.18})$$

In (C.4), it is imposed that the displacement value in the normal direction takes the same value for both materials in contact, $u_\theta^w(r, \vartheta) =$

$u_{\theta}^{w+1}(r, \vartheta)$, but this value is unknown and can be defined by applying the expression (C.18)₁ as

$$u_{\theta}^w(r, \vartheta_w) + u_{\theta}^{w+1}(r, \vartheta_w) = \mathbf{n}^T(\vartheta)\mathbf{u}^w(r, \vartheta_w) + \mathbf{n}^T(\vartheta)\mathbf{u}^{w+1}(r, \vartheta_w) = \mathbf{n}^T(\vartheta_w)\mathbf{u}^w(r, \vartheta_w) + \mathbf{0}_{1 \times 3}\boldsymbol{\varphi}^w(r, \vartheta_w) + \mathbf{n}^T(\vartheta_w)\mathbf{u}^{w+1}(r, \vartheta_w) + \mathbf{0}_{1 \times 3}\boldsymbol{\varphi}^{w+1}(r, \vartheta_w) = w_{\text{corner}_{U_1}} \tag{C.19}$$

and in matrix form

$$\begin{bmatrix} \mathbf{n}^T(\vartheta_w) & \mathbf{0}_{1 \times 3} & \mathbf{n}^T(\vartheta_w) & \mathbf{0}_{1 \times 3} \end{bmatrix} \begin{bmatrix} \mathbf{u}^w(r, \vartheta_w) \\ \boldsymbol{\varphi}^w(r, \vartheta_w) \\ \mathbf{u}^{w+1}(r, \vartheta_w) \\ \boldsymbol{\varphi}^{w+1}(r, \vartheta_w) \end{bmatrix} = w_{\text{corner}_{U_1}}. \tag{C.20}$$

It is known that the stress field must fulfil the Coulomb law, but the value of each component and, therefore, the value of the stress function vector is unknown. To determine the value of the stress function vector it is necessary to know its value corresponding to the $\mathbf{n}_{\mu}(\vartheta_w)$ direction. As the stress function value is the same in the wedges w and $w + 1$, expression (C.18)₂ is rewritten as

$$\begin{bmatrix} \mathbf{0}_{1 \times 3} & \mathbf{n}_{\mu}^T(\vartheta_w) & \mathbf{0}_{1 \times 3} & \mathbf{n}_{\mu}^T(\vartheta_w) \end{bmatrix} \begin{bmatrix} \mathbf{u}^w(r, \vartheta_w) \\ \boldsymbol{\varphi}^w(r, \vartheta_w) \\ \mathbf{u}^{w+1}(r, \vartheta_w) \\ \boldsymbol{\varphi}^{w+1}(r, \vartheta_w) \end{bmatrix} = w_{\text{corner}_{U_2}}. \tag{C.21}$$

As both the difference and the sum of the tangential resultant displacement in the $\mathbf{k}(\vartheta_w, \omega_k)$ direction are unknowns, expressions (C.18)₃ and (C.18)₄ respectively, the value of the displacement in the direction $\mathbf{k}(\vartheta_w, \omega_k)$ for wedge w is

$$\mathbf{k}^T(\vartheta_w, \omega_k)\mathbf{u}^w(r, \vartheta_w) = w_{\text{corner}_{U_3}}, \tag{C.22}$$

and in matrix form

$$\begin{bmatrix} \mathbf{k}^T(\vartheta_w, \omega_k) & \mathbf{0}_{1 \times 3} & \mathbf{0}_{1 \times 3} & \mathbf{0}_{1 \times 3} \end{bmatrix} \begin{bmatrix} \mathbf{u}^w(r, \vartheta_w) \\ \boldsymbol{\varphi}^w(r, \vartheta_w) \\ \mathbf{u}^{w+1}(r, \vartheta_w) \\ \boldsymbol{\varphi}^{w+1}(r, \vartheta_w) \end{bmatrix} = w_{\text{corner}_{U_3}}, \tag{C.23}$$

and similar for wedge $w + 1$,

$$\begin{bmatrix} \mathbf{0}_{1 \times 3} & \mathbf{0}_{1 \times 3} & \mathbf{k}^T(\vartheta_w, \omega_k) & \mathbf{0}_{1 \times 3} \end{bmatrix} \begin{bmatrix} \mathbf{u}^w(r, \vartheta_w) \\ \boldsymbol{\varphi}^w(r, \vartheta_w) \\ \mathbf{u}^{w+1}(r, \vartheta_w) \\ \boldsymbol{\varphi}^{w+1}(r, \vartheta_w) \end{bmatrix} = w_{\text{corner}_{U_4}}. \tag{C.24}$$

The last expression defines the displacement vector as the sum of the displacements in the $\mathbf{m}(r, \vartheta_w)$ direction (C.18)₅

$$\begin{bmatrix} \mathbf{m}(\vartheta_w, \omega_k) & \mathbf{0}_{1 \times 3} & \mathbf{m}(\vartheta_w, \omega_k) & \mathbf{0}_{1 \times 3} \end{bmatrix} \begin{bmatrix} \mathbf{u}^w(r, \vartheta_w) \\ \boldsymbol{\varphi}^w(r, \vartheta_w) \\ \mathbf{u}^{w+1}(r, \vartheta_w) \\ \boldsymbol{\varphi}^{w+1}(r, \vartheta_w) \end{bmatrix} = w_{\text{corner}_{U_5}}, \tag{C.25}$$

By collecting the previous expressions of unknown variables in (C.18) in matrix form, the matrices $\tilde{\mathbf{D}}_1$ and $\tilde{\mathbf{D}}_2$ in Table 2 are constructed by means of the expressions (C.20), (C.21) and (C.23)–(C.25), and once again adding a factor $\frac{1}{\sqrt{2}}$ or $\sqrt{2}$ to ensure their orthonormality.

References

[1] J.R. Barber, *Contact Mechanics*, Springer, Cham, 2018.
 [2] D. Leguillon, E. Sanchez-Palencia, *Computation of Singular Solutions in Elliptic Problems and Elasticity*, Masson, Paris, 1987.
 [3] Z. Yosibash, *Singularities in Elliptic Boundary Value Problems and Elasticity and their Connection with Failure*, Springer, New York, 2012.
 [4] J.P. Dempsey, G.B. Sinclair, On the stress singularities in the plane elasticity of the composite wedge, *J. Elast.* 9 (4) (1979) 317–327.

[5] G.B. Sinclair, Stress singularities in classical elasticity–I: Removal, interpretation and analysis, –II: Asymptotic identification, *Appl. Mech. Rev.* 57 (2004) 251–297, 385–439.
 [6] A.M. Linkov, V.F. Koshelev, Multi-wedge points and multi-wedge elements in computational mechanics: Evaluation of exponents and angular distribution, *Int. J. Solids Struct.* 43 (2006) 5909–5930.
 [7] A. Carpinteri, M. Paggi, Analytical study of the singularities arising at multi-material interfaces in 2D linear elastic problems, *Eng. Fract. Mech.* 74 (2007) 59–74.
 [8] M. Paggi, A. Carpinteri, On the stress singularities at multimaterial interfaces and related analogies with fluid dynamics and diffusion, *Appl. Mech. Rev.* 61 (2008) 020801–1–22.
 [9] C. Sator, W. Becker, Closed-form solutions for stress singularities at plane bi-and trimaterial junctions, *Arch. Appl. Mech.* 82 (5) (2012) 643–658.
 [10] T.C.T. Ting, Stress singularities at the tip of interfaces in polycrystals, in: H.P. Rossmannith (Ed.), *Damage and Failure of Interfaces*, Balkema Publishers, Rotterdam, 1997, pp. 75–82.
 [11] M. Costabel, M. Dauge, Y. Lafranche, Fast semi-analytic computation of elastic edge singularities, *Comput. Methods Appl. Mech. Engrg.* 190 (24) (2001) 2111–2134.
 [12] K.-C. Wu, Near-tip field and the associated path-independent integrals for anisotropic composite wedges, *J. Mech.* 17 (1) (2001) 21–28.
 [13] A. Barroso, V. Mantić, F. París, Singularity analysis of anisotropic multimaterial corners, *Int. J. Fract.* 119 (1) (2003) 1–23.
 [14] C. Hwu, M. Omiya, K. Kishimoto, A key matrix N for the stress singularity of the anisotropic elastic composite wedges, *JSME Int. J. Series A* 46 (2003) 40–50.
 [15] W.L. Yin, Anisotropic elasticity and multi-material singularities, *J. Elast.* 71 (2003) 263–292.
 [16] V. Mantić, F. París, J. Berger, Singularities in 2D anisotropic potential problems in multi-material corners. Real variable approach, *Int. J. Solids Struct.* 40 (2003) 5197–5218.
 [17] M. Steigemann, Power-law solutions of anisotropic multi-material elasticity problems, *J. Elast.* 118 (2015) 63–87.
 [18] M.A. Herrera-Garrido, V. Mantić, A. Barroso, A powerful matrix formalism for stress singularities in anisotropic multi-material corners. Homogeneous (orthogonal) boundary and interface conditions, *Theor. Appl. Fract. Mech.* 119 (103271) (2021).
 [19] T.A. Laursen, *Computational Contact and Impact Mechanics: Fundamentals of Modeling Interfacial Phenomena in Nonlinear Finite Element Analysis*, Springer Berlin, Heidelberg, 2003.
 [20] P. Wriggers, *Computational Contact Mechanics*, 2nd ed., Springer, Berlin, 2006.
 [21] V. Yastrebov, *Numerical Methods in Contact Mechanics*, IST/WILEY, London, 2013.
 [22] V.L. Popov, *Contact Mechanics and Friction. Physical Principles and Applications*, 2nd Ed., Springer, Berlin, 2017.
 [23] M. Comninou, Stress singularity at a sharp edge in contact problems with friction, *Z. Angew. Math. Phys. ZAMP* 27 (1976) 493–499.
 [24] M. Comninou, Interface crack with friction in the contact zone, *J. Appl. Mech.* 44 (4) (1977) 780–781.
 [25] M. Comninou, J. Dundurs, A closed crack tip terminating at an interface, *J. Appl. Mech.* 46 (1979) 97–100.
 [26] A.C. Wijeyewickrema, J. Dundurs, L.M. Keer, The singular stress field of a crack terminating at a frictional interface between two materials, *J. Appl. Mech.* 62 (2) (1995) 289–293.
 [27] C.M. Churchman, D.A. Hills, General results for complete contacts subject to oscillatory shear, *J. Mech. Phys. Solids* 54 (2006) 1186–1205.
 [28] R. Arias, R. Madariaga, M. Adda-Bedia, Singular elasto-static field near a fault kink, *Pure Appl. Geophys.* 168 (2011) 2167–2179.
 [29] Y.Y. Yang, Solutions of dissimilar material contact problems, *Eng. Fract. Mech.* 100 (2013) 92–107.
 [30] K. Hong, M.D. Thouless, W. Lu, J.R. Barber, Asymptotic stress fields for complete contact between dissimilar materials, *J. Appl. Mech.* 86 (2018) 011009.
 [31] P. Poonsawat, A.C. Wijeyewickrema, P. Karasudhi, Singular stress fields of angle-ply and monoclinic bimaterial wedges, *Int. J. Solids Struct.* 38 (2001) 91–113.
 [32] V. Magnier, S. Géry, D. Suzanne, Asymptotic approach to analyze singular stress state in anisotropic multi-material: Application to the rivets, *Int. J. Solids Struct.* 47 (16) (2010) 2070–2080.
 [33] D. Leguillon, Interface crack tip singularity with contact and friction, *CR Acad Sci, Ser IIb: Mec, Phys, Astron* 327 (1999) 437–442.
 [34] T.C.T. Ting, S.C. Chou, Stress singularities at tip of contact zone in anisotropic interface crack, in: A.R. Bunsell (Ed.), *First European Conference on Composite Materials (ECCM1)*, European Association for Composite Materials, Bordeaux, 1985, pp. 164–169.
 [35] J.C. Sung, W.G. Chung, Frictional interface crack in anisotropic bimaterial under combined shear and compression, *Int. J. Solids Struct.* 40 (2003) 6839–6857.
 [36] H.-P. Chen, Z. Guo, X. Zhou, Stress singularities of contact problems with a frictional interface in anisotropic bimaterials, *Fat. Fract. Eng. Mater. Struct.* 35 (2012) 718–731.

- [37] V. Mantič, A. Barroso, F. París, Singular elastic solutions in anisotropic multi-material corners. Applications to composites, in: V. Mantič (Ed.), *Mathematical Methods and Models in Composites*, Imperial College Press, 2014, pp. 425–495.
- [38] V. Mantič, A. Barroso, F. París, Computational procedure for singularity analysis of anisotropic elastic multimaterial corners- Applications to composites and their joints, in: V. Mantič (Ed.), *Mathematical Methods and Models in Composites (Second Edition)*, World Scientific, 2023, pp. 613–695.
- [39] A.N. Stroh, Dislocations and cracks in anisotropic elasticity, *Philos. Mag.* 3 (1958) 625–646.
- [40] A.N. Stroh, Steady state problems in anisotropic elasticity, *J. Math. Phys.* 41 (1962) 77–103.
- [41] T.C.T. Ting, *Anisotropic Elasticity, Theory and Applications*, Oxford University Press, New York, 1996.
- [42] C. Hwu, *Anisotropic Elastic Plates*, Springer, New York, 2010.
- [43] V. Mantič, F. París, J. Cañas, Stress singularities in 2D orthotropic corners, *Int. J. Fract.* 83 (1997) 67–90.
- [44] G.H. Golub, C.F. Loan, *Matrix Computations*, The Johns Hopkins University Press, Baltimore, 1985.
- [45] M.L. Williams, The stresses around a fault or crack in dissimilar media, *Bull. Seismol. Soc. Am.* 49 (1959) 199–204.
- [46] A.H. England, A crack between dissimilar media, *J. Appl. Mech.* 32 (1965) 400–402.
- [47] E.E. Gdoutos, P.S. Theocaris, Stress concentrations at the apex of a plane indenter acting on an elastic half plane, *J. Appl. Mech.* 42 (1975) 688–692.
- [48] M.L. Williams, Stress singularities resulting from various boundary conditions in angular corners of plates in extension, *J. Appl. Mech.* 19 (1952) 526–528.
- [49] M.A. Herrera-Garrido, V. Mantič, A semi-analytic procedure for stress singularities in anisotropic bimaterial corners with frictional contact, 2024, under review.
- [50] M. Comninou, The interface crack, *J. Appl. Mech.* 44 (1977) 631–636.
- [51] M.A. Herrera-Garrido, V. Mantič, Stress singularities in the generalised Comninou frictional contact model for interface cracks in anisotropic bimaterials, 2024, under review.
- [52] A.K. Head, The Galois unsolvability of the sextic equation of anisotropic elasticity, *J. Elast.* 9 (1979) 9–20.
- [53] Z. Mróz, S. Stupkiewicz, An anisotropic friction and wear model, *Int. J. Solids Struct.* 31 (8) (1994) 1113–1131.
- [54] L. Rodríguez-Tembleque, R. Abascal, M.H.F. Aliabadi, Anisotropic wear framework for 3D contact and rolling problems, *Comput. Methods. Appl. Mech. Eng.* 241–244 (2012) 1–19.
- [55] J. Allo, Implementación de un código para el cálculo de singularidad de tensiones en esquinas multimateriales anisótropas, (Master's Thesis), Universidad de Sevilla, Departamento de Mecánica de Medios Continuos, Teoría de Estructuras e Ingeniería del Terreno. Universidad de Sevilla, 2013.
- [56] V.A. Kondratiev, Boundary problems for elliptic equations in domains with conical or angular points, *Trans. Moscow Math. Soc.* 16 (1967) 227–313.
- [57] M. Costabel, M. Dauge, Construction of corner singularities for Agmon-Douglis-Nirenberg elliptic systems, *Math. Nachr.* 162 (1) (1993) 209–237.